

Review

One-Dimensional Zinc Oxide Nanomaterials for Application in High-Performance Advanced Optoelectronic Devices

Meng Ding ^{1,2}, Zhen Guo ^{2,*}, Lianqun Zhou ^{2,*} , Xuan Fang ³, Lili Zhang ⁴, Leyong Zeng ⁵, Lina Xie ³ and Hongbin Zhao ^{6,*}

¹ School of Physics and Technology, University of Jinan, 336 Nanxinzhuang West Road, Jinan 250022, China; dingmeng0207@163.com

² CAS Key Lab of Bio-Medical Diagnostics, Suzhou Institute of Biomedical Engineering and Technology, Chinese Academy of Sciences, Suzhou 215163, China

³ School of Science and Engineering, The Chinese University of Hong Kong, Shenzhen 518172, China; fangxuan110@hotmail.com (X.F.); linna.xie@madison-tech.com (L.X.)

⁴ Shanghai Synchrotron Radiation Facility, Shanghai Institute of Applied Physics, Chinese Academy of Sciences, 239 Zhangheng Rd., Pudong, Shanghai 201800, China; zhanglili@sinap.ac.cn

⁵ College of Chemistry & Environmental Science, Hebei University, Baoding 071002, China; zengly@hbu.edu.cn

⁶ State Key Laboratory of Advanced Materials for Smart Sensing, General Research Institute for Nonferrous Metals, Beijing 100088, China

* Correspondence: guozhen@sibet.ac.cn (Z.G.); zhoulq@sibet.ac.cn (L.Z.); zhaohongbin@grinm.com (H.Z.)

Received: 27 April 2018; Accepted: 13 May 2018; Published: 18 May 2018



Abstract: Unlike conventional bulk or film materials, one-dimensional (1D) semiconducting zinc oxide (ZnO) nanostructures exhibit excellent photoelectric properties including ultrahigh intrinsic photoelectric gain, multiple light confinement, and subwavelength size effects. Compared with polycrystalline thin films, nanowires usually have high phase purity, no grain boundaries, and long-distance order, making them attractive for carrier transport in advanced optoelectronic devices. The properties of one-dimensional nanowires—such as strong optical absorption, light emission, and photoconductive gain—could improve the performance of light-emitting diodes (LEDs), photodetectors, solar cells, nanogenerators, field-effect transistors, and sensors. For example, ZnO nanowires behave as carrier transport channels in photoelectric devices, decreasing the loss of the light-generated carrier. The performance of LEDs and photoelectric detectors based on nanowires can be improved compared with that of devices based on polycrystalline thin films. This article reviews the fabrication methods of 1D ZnO nanostructures—including chemical vapor deposition, hydrothermal reaction, and electrochemical deposition—and the influence of the growth parameters on the growth rate and morphology. Important applications of 1D ZnO nanostructures in optoelectronic devices are described. Several approaches to improve the performance of 1D ZnO-based devices, including surface passivation, localized surface plasmons, and the piezo-phototronic effect, are summarized.

Keywords: zinc oxide; one-dimensional nanostructure; light-emitting diode; photodetector; localized surface plasmon; piezo-phototronic effect

1. Introduction

The small size of one-dimensional (1D) nanomaterials leads to unique electrical, mechanical, chemical, and optical properties that are attractive for application in nanoscience and nanotechnology.

In particular, 1D zinc oxide (ZnO) is a representative nanomaterial with excellent properties, such as ultrahigh intrinsic photoelectric gain and multiple array light confinement. Thus, ZnO nanomaterials have been well studied in recent years with the goal of constructing advanced optoelectronic devices with improved performance [1]. It is anticipated that 1D ZnO nanomaterials could be used as an important basic unit of nanostructured systems. Several types of 1D ZnO nanostructures have been reported, including nanowires [2–6], nanorods [7–9], nanobelts [10–13], and nanotubes [14–16]. Considering actual application requirements, 1D ZnO nanomaterials are usually considered an ideal medium to construct optoelectronic devices. The performance of optoelectronic devices could be improved using 1D ZnO nanomaterials because of their excellent properties, such as carrier transport with high mobility, efficient light confinement, and light emission. Thus, 1D ZnO nanowires are usually used in devices for applications such as light emission, photon detection, and biochemical sensing. In addition, nanowire-like structures could be considered as an ideal system for physical studies investigating the carrier transport, light confinement, and energy loss behaviors of 1D confined objects. Therefore, 1D ZnO nanowires are favorable not only for examining the basic phenomena of low-dimensional systems, but also for constructing new types of nanodevices that exhibit high performance.

As a member of the II-VI family, ZnO possesses properties such as a wide direct band gap of 3.37 eV, large exciton binding energy of 60 meV at room temperature, and suitable features for feasible production of nanomaterials. Potential applications of ZnO materials include optical waveguides [17], varistors [18], solid-state lighting [19], gas sensors [20], and transparent conductive films. Because of its wide band gap, ZnO is a promising candidate material for use in solid-state optoelectronics that emit in the blue or ultraviolet (UV) spectral range, including lasers. In addition, the large exciton binding energy of ZnO means that it can display efficient excitonic emission even at room temperature [21].

Various fabrication methods of 1D ZnO nanomaterials have been developed, such as vapor transport [5], hydrothermal reaction [8,11,16,22], electrodeposition [12,23], chemical vapor deposition (CVD) [24,25], molecular beam epitaxy [26], and pulsed laser deposition [27]. These methods can be used to obtain samples on substrates such as Si, quartz, and sapphire. Each method has its specific merits and inevitable weaknesses. The gas vapor approaches can fabricate high-quality single-crystalline ZnO nanostructures. However, these processes require high temperatures (about 450–1000 °C) and often have other limitations, including poor sample uniformity, narrow substrate choice, and low product yield. Solution processing is one of the most commonly used methods to prepare 1D ZnO nanomaterials because of its low cost, controllability, and compatibility with large-area manufacturing.

Compared with other 1D nanomaterials, ZnO has three prominent advantages: first, it is a semiconductor with a piezoelectric effect, which is the basis for electric mechanical coupling sensors and inverters; second, the biosecurity and biocompatibility of ZnO is relatively high, so it can be used in medicine; third, ZnO has the largest range of known nanostructures, including nanowires [2–6], nanorods [7–9], nanobelts [10–13], nanotubes [14–16], nanoplates [28–30], nanospheres [31], nanotrees [32], nanoleaves [33], and nanosails [34]. In addition, ZnO tetrapod [35], microrod/microwire [36,37], porous array [38], matrix [39], and 3D network nanostructure [20,40] have been obtained. At present, many researchers are focusing on constructing devices based on ZnO nanomaterials. New devices based on 1D ZnO nanomaterials are constantly being developed, such as room-temperature lasers, light-emitting diodes (LEDs), photodetectors, sensors, and transistors. These devices containing 1D ZnO nanomaterials exhibit better performance than that of devices with thin films and bulk materials. The excellent performance of new devices based on 1D ZnO nanomaterials reveal their great potential for applications in many fields.

Previously, there were some review articles about ZnO nanostructure, for example, Wang et al. reviewed various nanostructures of ZnO using solid-vapor phase technique, growth mechanisms, the application of nanobelts in nanosensors, field effect transistors, and nanoresonators [1]. Yi et al., reviewing the fabrication method and doping of ZnO nanorods, also discussed the properties

related to ZnO nanorods, including luminescence, field emission, electron transport, as well as various applications [41]. Wang comprehensively reviewed various ZnO nanostructures fabricated by wet chemical methods, their doping and alloying, patterned growth, application in catalysis, surface modification, sensing, optoelectronic, and so on [42]. The review mainly focuses on the effect of growth conditions on 1D ZnO nanostructures and achievements of 1D ZnO-based photodetectors and LEDs, and, in particular, the promising approaches to improve the performance of LEDs and photodetectors.

In this review, we briefly introduce the properties of ZnO, review the growth methods of 1D ZnO nanomaterials, and describe the progress and current status of photoelectric devices (LEDs and photodetectors) based on 1D ZnO nanomaterials. Section 2 provides a brief introduction to the basic properties of 1D ZnO nanostructures. Section 3 covers the fabrication of 1D ZnO nanostructures, including CVD, hydrothermal reaction, and electrodeposition, and describes the influence of growth parameters on the growth rate and morphology of 1D ZnO nanostructures. Finally, we focus on LEDs and photodetectors based on 1D ZnO nanomaterials. The recent achievements of ZnO-based photodetectors and LEDs with different device structures and promising approaches to improve the performance of LEDs and photodetectors—including surface passivation, localized surface plasmons resonance (LSPR), and the piezo-phototronic effect—are discussed.

2. Basic Properties of ZnO

ZnO is II-VI compound semiconductor with direct wide band gap of 3.37 eV at room temperature. ZnO has three typical crystal structures: wurtzite, zinc blende, and rock salt. The thermodynamically stable phase of ZnO at ambient temperature and pressure is wurtzite. The zinc blende structure can be stabilized by growth on cubic substrates. The rock-salt structure can be fabricated at high pressure [21].

Wurtzite ZnO has a hexagonal structure with lattice parameters a and c and belongs to the $P6_3mc$ space group. The lattice parameter a mostly ranges from 0.32475 to 0.32501 nm, and c typically ranges from 0.520642 to 0.52075 nm [43]. The deviation of ZnO lattice constants from the ideal values is probably caused by the presence of point defects, such as zinc antisites, oxygen vacancies, and dislocations [21]. As illustrated in the schematic of the wurtzite ZnO structure shown in Figure 1, both Zn and O atoms arrange in a hexagonal close-packed (hcp) pattern and are stacked alternately along the c -axis. Furthermore, each kind of atom is surrounded by four atoms of the other kind, and the O^{2-} or Zn^{2+} of two adjacent layers form a tetrahedral structure. The resulting non-centrosymmetric structure of wurtzite ZnO can result in piezoelectricity and the thermoelectric effect. A ZnO single crystal exhibits very strict crystallographic polarity. The polar plane of such a crystal is the basal plane, which is composed of the Zn (0001) plane and O (000 $\bar{1}$) plane, inducing a normal dipole moment, spontaneous polarization along the c -axis, and a distinct surface energy [1,21].

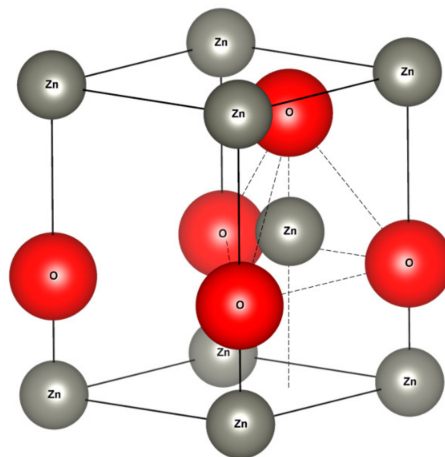


Figure 1. Schematic illustration of the wurtzite ZnO structure.

3. Growth of ZnO Nanostructures

ZnO probably possesses the richest variety of reported nanostructures, which are typically categorized into three groups: zero-dimensional, 1D, and two-dimensional. The four most common types of 1D ZnO nanostructures are nanowires [2–6], nanorods [7–9], nanobelts [10–13], and nanotubes [14–16]. Many approaches have been used to fabricate 1D ZnO nanostructures, such as CVD [4–6], hydrothermal processing [8,11,16,22], electrochemical deposition [12,23], and magnetron sputtering [44], with and without a catalyst.

3.1. Chemical Vapor Deposition

CVD is the one most commonly used methods to synthesize 1D ZnO nanostructures. In the CVD synthesis process, ZnO powder, Zn powder, or another Zn compound is used as the raw material after evaporation, reduction/oxidation, decomposition/combination, and other physical and chemical changes. The growth process is commonly carried out in a horizontal tube furnace, which consists of a horizontal tube heater, an alumina or quartz tube, a gas supply, and a control system. The fabrication of 1D ZnO nanostructures by CVD is generally affected by the synthesis parameters, such as the growth temperatures of the source and substrate, the distance between the source and substrate, heating rate, carrier gas (including gas species and flow rate), tube diameter, pressure, and atmosphere. Usually, the vapor–liquid–solid (VLS) process is used for 1D ZnO nanostructure growth via CVD, which requires a catalyst such as gold (Au) [5], copper (Cu) [45], stannum (Sn) [46], or cobalt (Co) [47]. The liquid droplet serves as a preferential site for absorption of the gas-phase reactant until the droplet is saturated and then becomes the nucleation site for crystallization. During growth, the catalyst droplet regulates the growth direction and controls the diameter of the nanowire [1]. Control of the nanowire diameter has also been achieved by varying the Au layer thickness. As shown in Figure 2, when the Au film coated on a substrate was 5 nm thick, the ZnO nanowires had diameters of 80–120 nm and lengths of 10–20 μm . When the Au film was 3 nm thick, the ZnO nanowires had diameters of 40–70 nm and lengths of 5–10 μm [5]. In addition to using external catalysts, Zn itself can act as a catalyst under certain conditions to prepare 1D ZnO nanostructures [48].

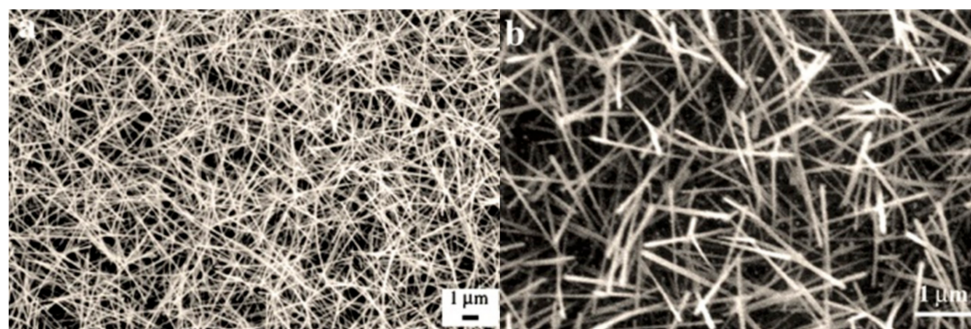


Figure 2. Scanning electron microscopy (SEM) images of ZnO nanowires grown on silicon substrates coated with gold films with a thickness of (a) ~5 nm and (b) 3 nm [5]. Reproduced with permission.

The influence of different catalyst thin films on the morphology and even nucleation process of ZnO nanomaterials varies. Osgoods et al. systematically studied ZnO nanowire growth using diverse metal catalysts (Au, Ag, Ni, and Fe) and substrates (Si, sapphire) with different structures and crystal orientation. SEM images of the nanowires are shown in Figure 3 [41–49]. The ZnO nanowires grew through the vapor–solid mechanism in the case of an iron (Fe) catalyst and via the VLS process using Au, Ag, or Ni as the catalyst. The ZnO nanostructures grown using different catalysts possessed differences in not only size and the ratio of length to diameter, but also the atomic composition ratio of Zn to O. Thus, the relative intensity of the oxygen vacancy-related emission in photoluminescence spectra of nanostructures grown on different thin films varied.

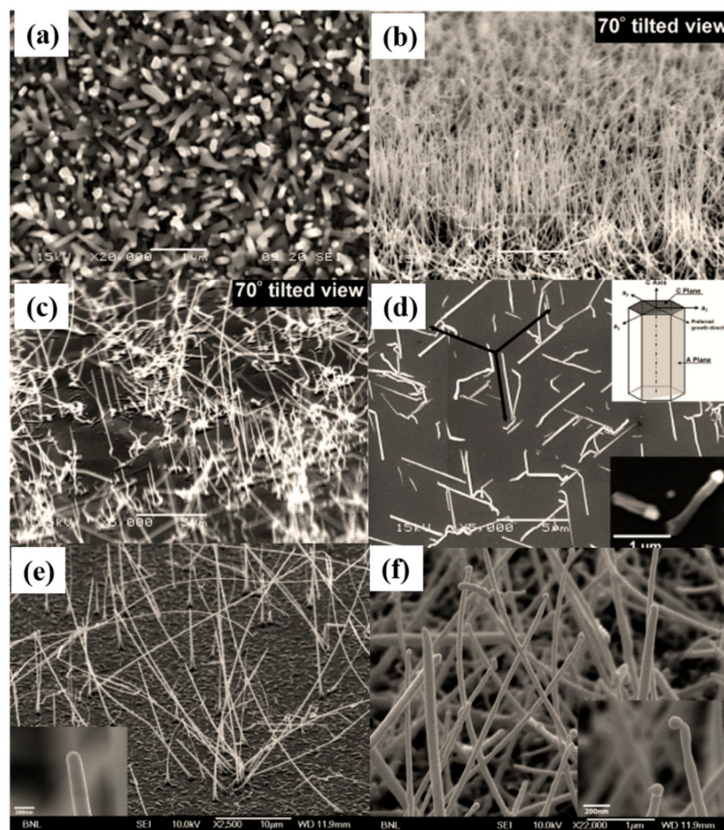


Figure 3. SEM images of ZnO nanowires fabricated on (a) Au-coated Si (111) and (b) Au-coated a-plane sapphire; (c) a-plane (110) sapphire coated with a 2.5 nm Ag film and (d) c-plane (001) sapphire coated with a 2.5 nm Ag thin film. SEM images (tilt angle of 60°) of ZnO nanowires grown on (e) an a-plane (110) sapphire substrate coated with a 2.5 nm Fe thin film and (f) a-plane sapphire with a 2.5 nm Ni thin film [49]. Reproduced with permission.

A ZnO thin film or other transition layer can be prepared on the substrate to facilitate the nucleation growth of 1D ZnO nanostructures. Fang et al. [6] demonstrated that ZnO thin films fabricated by electron-beam evaporation can provide nucleation sites to control the growth direction of ZnO nanowires. In addition, the density of ZnO nanowires could be adjusted by varying the thickness of the ZnO thin film, as shown in Figure 4. Yang and coworkers fabricated radial ZnO nanowire arrays on Si substrates with an amorphous carbon thin layer without a metal catalyst [50].

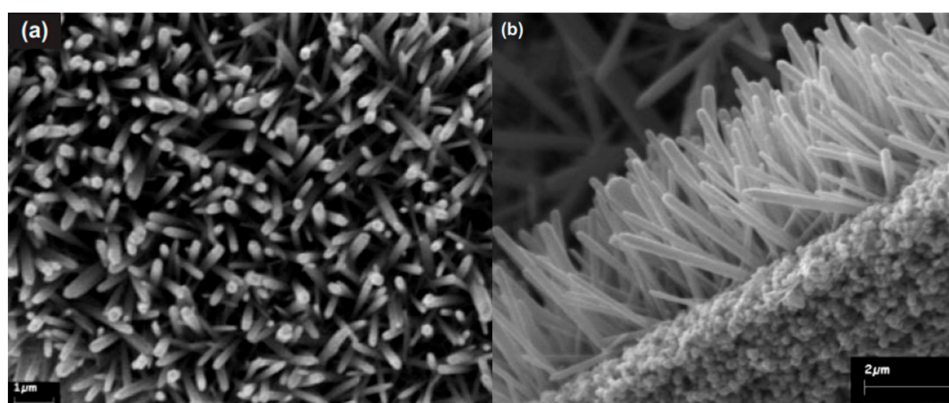


Figure 4. SEM images of ZnO nanorods grown on (a) a silicon wafer and (b) a ZnO nanostructured thin film [2]. Reproduced with permission.

3.2. Hydrothermal Method

The hydrothermal method is a very powerful technique for the growth of 1D ZnO nanomaterials, which involves chemical reaction of substances in solution at a certain temperature and pressure to fabricate the nanomaterials. This technique enables the synthesis of most materials with the required physical and chemical properties. Compared with other conventional preparation methods, the hydrothermal method has many advantages, such as low cost, simplicity, limited pollution, good nucleation and shape control, and low-temperature (<200 °C) growth at higher pressure in the presence of an appropriate solvent. In addition, the size distribution of materials obtained by the hydrothermal technique is uniform, with hardly any aggregation. The shape and size of the prepared materials are influenced by several processing parameters, such as the molar ratio and concentration of the reactant, temperature, and reaction time.

Vayssieres et al. [2,51] first used the hydrothermal method to fabricate ZnO nanorods in 2001. Equimolar mixed solutions of zinc nitrate ($\text{Zn}(\text{NO}_3)_2$) and hexamethylenetetramine ($\text{C}_6\text{H}_{12}\text{N}_4$, HMT) with different concentrations (1–10 mM) were heated at a constant temperature of 95 °C for several hours. The products were cleaned and then dried to give ZnO nanorod arrays. Various materials were used as substrates in their hydrothermal growth of ZnO nanostructures; for example, polycrystalline fluorine-doped tin oxide (FTO)-coated glass, single-crystalline sapphire, and Si/SiO₂ wafers with ZnO thin films. The experiments showed that the diameter of ZnO nanorods was controlled by the concentration of the precursors. As the concentration of the solution was lowered from 10 to 1 mM, the diameter of the nanorods decreased from 100–200 nm to 10–20 nm. SEM images of the ZnO nanorods fabricated by the hydrothermal method are shown in Figure 4. In this approach, only two kinds of chemical solutions with good solubility are needed. The two solutions can readily mix uniformly and promote ZnO formation, greatly simplifying and lowering the cost of the experimental process. The simple setup for hydrothermal growth of ZnO nanostructures is also beneficial to improve the purity of products and study the influence of synthetic parameters on nanostructure formation.

The method developed by Vayssieres and colleagues has since been greatly improved and remains in common use because of its simplicity. To improve the quality of the product and the controllability of the deposition process, a crystalline seed layer can be prepared on the substrate prior to hydrothermal growth. In 2003, Yang's group grew uniform ZnO nanowires on various substrates (e.g., Si (100) wafers and flexible polydimethylsiloxane films) using a two-step hydrothermal method [52]. The first step involved the preparation of a seed layer of ZnO nanocrystals with a diameter of 5–10 nm, which were spin-cast several times on the substrate to give a seed-layer thickness of 50–200 nm. The second step was ZnO nanowire growth by the hydrothermal method. The substrate with a seed crystal layer was placed in an open crystallizing dish filled with an equimolar solution of zinc nitrate hydrate and methenamine or diethylenetriamine (0.025 M) at 90 °C. Other research groups have prepared seed crystals using techniques such as pulsed laser deposition [14], magnetron sputtering [53], the sol-gel method [22,54], and atomic layer deposition [55]. Using small, homogeneous ZnO nanocrystals as a seed layer can provide nanowires that are small in diameter, well aligned, and in intimate contact with the substrate. In addition, the existing seeds could bypass the nucleation step, promoting growth on the seeds rather than nucleation in the homogeneous bulk solution. ZnO nanowires tend to grow wherever there are ZnO seeds; therefore, the density of nanowires is usually quite high [42]. As a result, the density of ZnO nanowires can be controlled by the thickness of the seed layer [22].

Although it is practical and effective to prepare ZnO nanostructures by the hydrothermal method using $\text{Zn}(\text{NO}_3)_2$ and HMT as raw materials, this approach does have shortcomings. For example, it is difficult to obtain ZnO nanomaterials with a large ratio of length to diameter. To increase the aspect ratio of the ZnO nanostructures, poly(ethylenimine) can be added to the reaction solution [56]. The addition of a low concentration of sodium citrate can alter the morphology of the ZnO nanorods. Sun et al. [57] prepared ZnO nanorods via cetyltrimethylammonium bromide (CTAB)-assisted hydrothermal oxidation of Zn metal at 180 °C. CTAB played important roles in the growth of ZnO nanorods, affecting the erosion process and growth orientation.

Kim et al. [8] prepared single-crystalline vertically aligned ZnO nanorod arrays on various substrates (Si, SiO₂, and FTO glass) using a polymer-templated hydrothermal method at a low temperature of 93 °C. To ensure that the ZnO nanorods grew along the c-axis [0001] direction and to minimize the crystal mismatch with the substrate, a c-oriented ZnO seed layer was first fabricated by the sol-gel method. The morphologies of the resulting nanostructures could be transformed from rodlike to pencil-like, needle-like, tubelike, treelike, and spherelike by exploiting the structural polarity of the ZnO nanorods and adjusting the growth parameters, including the seed layer, pH, and temperature, as summarized in Figure 5. Thus, Kim and coworkers developed a simple process to obtain ZnO nanorods with controllable size, density, and lattice.

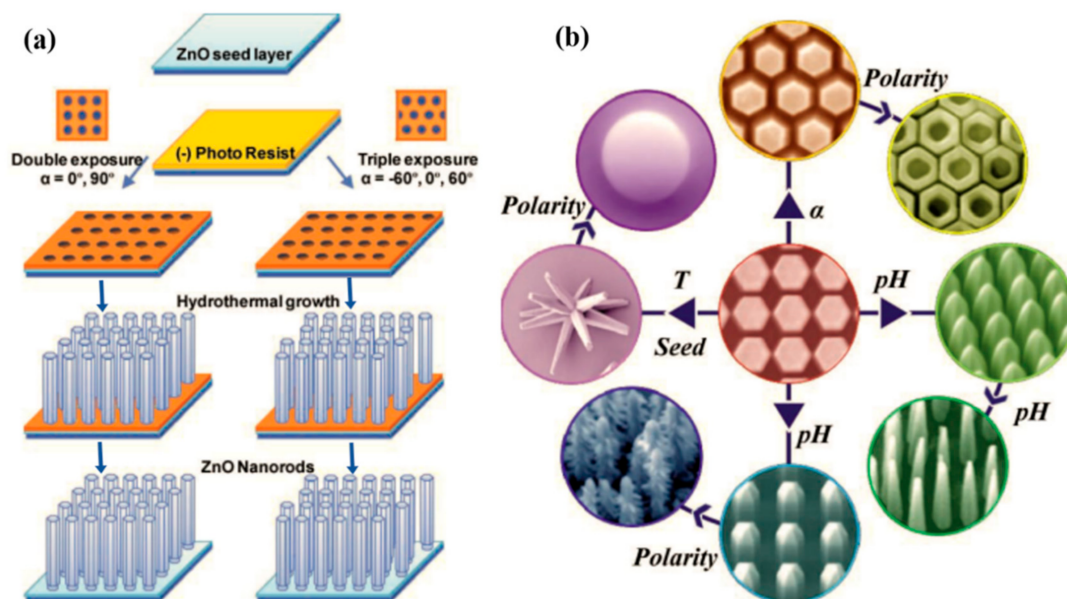


Figure 5. (a) Overview of the preparation process of periodic ZnO nanorods on various substrates (Si (100), SiO₂, and FTO glass); (b) high-resolution SEM images of the various ZnO nanostructures obtained using different reaction parameters [8]. Reproduced with permission.

3.3. Electrochemical Deposition

Electrochemical deposition has been widely used to obtain uniform and large-area growth of ZnO nanostructures [58]. Electrochemical deposition has many advantages, such as scalability, low cost, and easy handling [59]. Compared with ordinary chemical solution methods (e.g., hydrothermal methods), electrochemical deposition includes an external driving electric field in the reaction process, thus promoting reactions that are otherwise nonspontaneous. A standard three-electrode system with a saturated Ag/AgCl electrode as the reference electrode, Pt as the counter electrode (anode), and growth substrate as the working electrode is the typical setup for electrochemical deposition. In this case, the substrate serves as the cathode, so it must be conductive regardless of whether it is flat or curved. The substrate cathode is placed parallel to the anode in an aqueous solution of zinc salt (electrolyte). The chemical reaction is carried out in an electrolytic cell placed in a water bath to maintain a constant temperature.

Various groups have fabricated 1D ZnO nanostructures on FTO [60,61], indium-doped tin oxide (ITO) [62], polycrystalline Zn foil [63], and Si [64] substrates. Mari et al. [65] studied the influence of the bath temperature, current density, and deposition time on the growth rate of ZnO nanorods. Their results showed that the length of the nanorods increased with the current density and deposition time. Temperature had the opposite effect: the nanorods were longer when the deposition temperature was low. Xu and coworkers investigated the morphological control of ZnO nanostructures induced by addition of different capping agents, such as potassium chloride (KCl), ammonium fluoride (NH₄F),

ammonium acetate ($\text{CH}_3\text{COONH}_4$), and ethylenediamine (EDA) [62]. The morphology of the ZnO structures evolved from hexagonal rods to rhombohedral rods and woven nanoneedles upon varying the compositions of the mixed capping agents, as depicted in Figure 6.

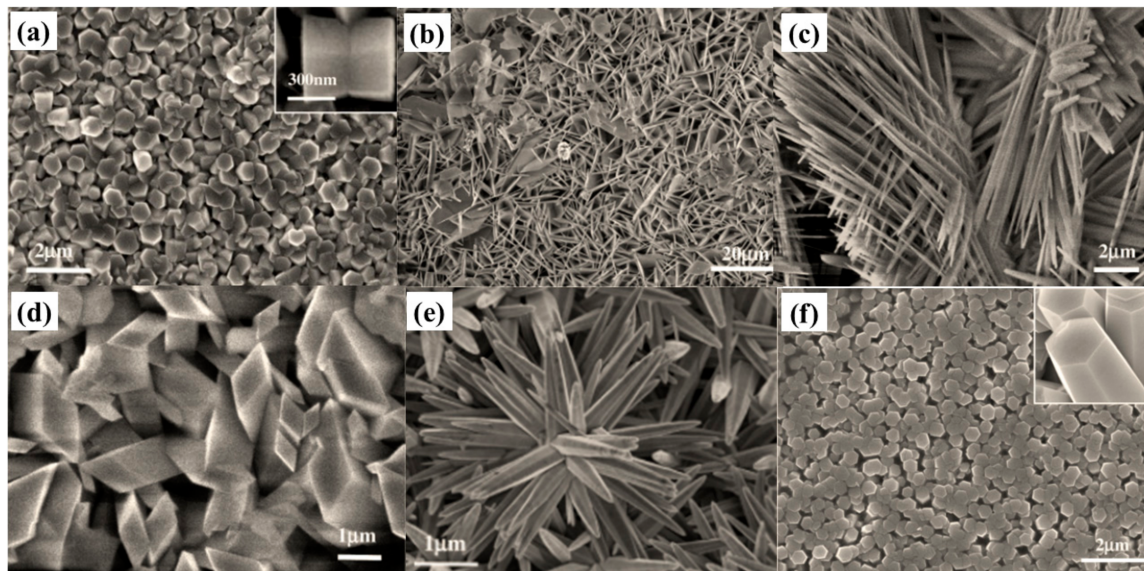


Figure 6. SEM images of the ZnO nanostructures formed by electrochemical deposition in solutions containing (a) 0.05 M $\text{Zn}(\text{NO}_3)_2$; (b) 0.05 M $\text{Zn}(\text{NO}_3)_2$ + 0.06 M KCl; (c) 0.05 M $\text{Zn}(\text{NO}_3)_2$ + 0.02 M NH_4F ; (d) 0.05 M $\text{Zn}(\text{NO}_3)_2$ + 0.2 M NH_4F ; (e) 0.05 M $\text{Zn}(\text{NO}_3)_2$ + 0.013 M ethylenediamine (EDA); and (f) 0.05 M $\text{Zn}(\text{NO}_3)_2$ + 0.06 M KCl + 0.01 M EDA [62]. Reproduced with permission.

Generally, zinc chloride (ZnCl_2) is used as the Zn^{2+} precursor when ZnO is deposited from the reduction of O_2 or H_2O_2 . Zaera et al. [66] examined the effect of chloride (Cl^-) concentration, which was mainly supplied by the KCl supporting electrolyte, on the mechanism of ZnO nanowire growth driven by O_2 reduction. The rate of oxygen reduction decreased with rising Cl^- concentration, and the deposition rate and dimensions of ZnO nanowire arrays could be tuned by varying the Cl^- concentration of the solution, as shown in Figure 7. The effect of different anions (Cl^- , SO_4^{2-} , and CH_3COO^-) on the reduction of dissolved O_2 in the deposition solution has also been studied [67]. The observed differences in the O_2 reduction rate were explained by the different adsorption behaviors of the anions. Therefore, the different adsorption behaviors of the anions on ZnO surfaces could affect the generation rate of hydroxide ions and influence the morphology and growth rate of the ZnO nanowires. It was also demonstrated that the diameter and length of ZnO nanowires could be adjusted by varying the type of anions in the deposition solution. In particular, the nanowires grown in the presence of Cl^- and CH_3COO^- possessed low and high aspect ratios, respectively.

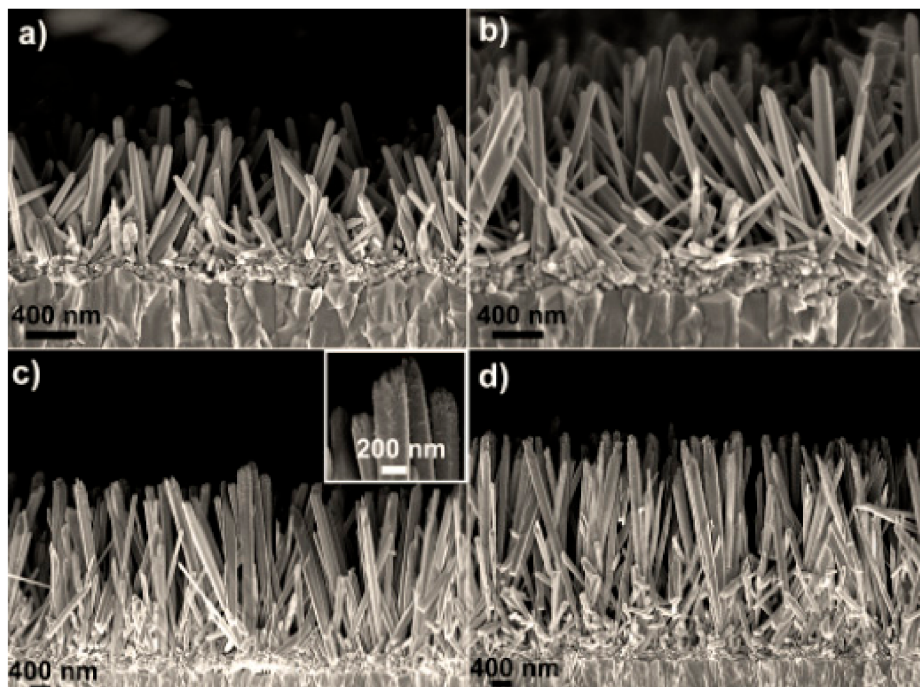


Figure 7. Cross-sectional SEM images of ZnO nanowire arrays obtained by electrochemical deposition using KCl concentrations of (a) 5×10^{-2} M; (b) 1 M; (c) 2 M; and (d) 3.4 M [66]. Reproduced with permission.

ZnO nanowires can also be fabricated by electrochemical deposition assisted by templates, including anodic aluminum oxide (AAO) [68–70], polycarbonate membranes [71,72], and porous films. AAO templates are widely used in the preparation of ZnO nanowires because of their simplicity and suitability for large-area, well-distributed nanowire fabrication. AAO templates can be prepared through a two-step anodization process [68,70]. The AAO template can be removed after nanowire growth, leaving the free-standing nanowires. Yi et al. [68] synthesized Zn nanowires consisting of the wurtzite hcp-Zn phase by electrodeposition on an AAO template with nanometer-sized pores. ZnO nanowires were then obtained by annealing the Zn nanowires at different temperatures for 10 h. Research has shown that this technique can provide not only ZnO nanowires, but also other semiconductor oxide nanostructures. However, ZnO and Al_2O_3 are amphoteric oxides, which makes the selective removal of the AAO membrane from the ZnO nanowires difficult. Polycarbonate membrane templates can be easily dissolved in chloroform, which makes them attractive to prepare free-standing 1D ZnO nanostructures. Wang and colleagues fabricated randomly distributed ZnO nanowires using a polycarbonate template [71]. Zeng et al. fabricated ZnO nanowire lines and bundle arrays on polystyrene (PS) template, as shown in Figure 8. The density of ZnO nanowires on Si substrate with 200 nm PS sphere template has decrease tendency with the heating time [73].

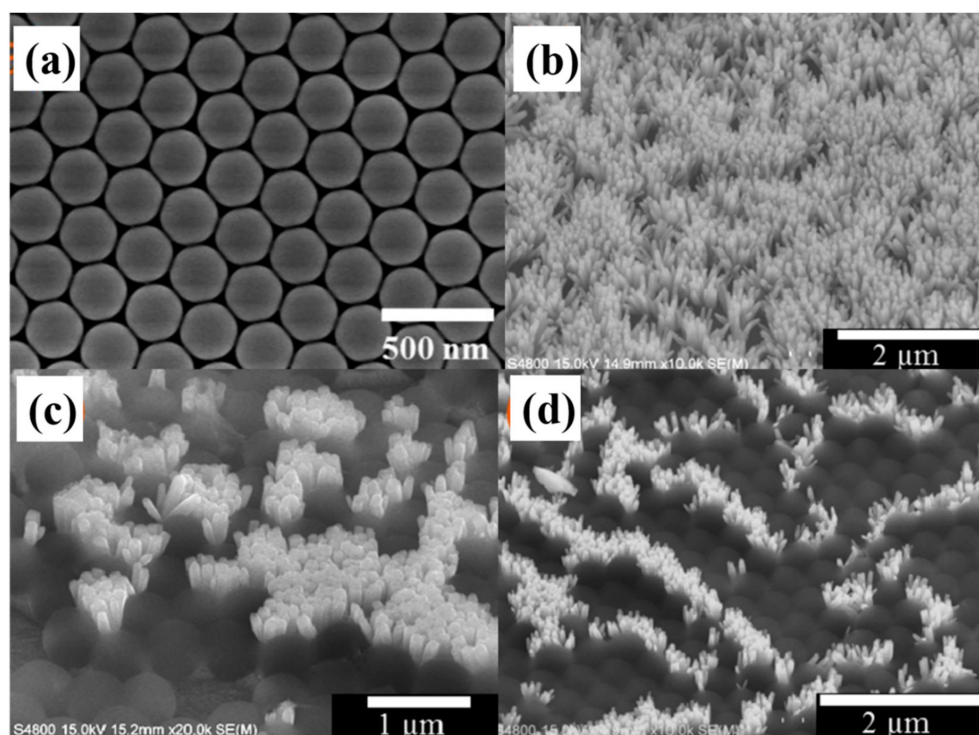


Figure 8. SEM images of 200 nm polystyrene (PS) sphere monolayer templates (a) and ZnO nanowires grown on 200 nm PS sphere template with heating time of 0 min (b); 3 min (c); 5 min (d), respectively [73]. Reproduced with permission.

4. Applications of 1D ZnO Nanostructures

4.1. Light-Emitting Diodes

An important feature of 1D ZnO nanomaterials is their excellent light transmission characteristics, which makes them attractive for use in high-efficiency UV LEDs and laser devices. ZnO nanomaterials display a direct wide band gap and large exciton binding energy at room temperature. UV LEDs have practical applications in solid-state lighting, UV photolithography, high-density data storage, and biomedical analysis [74]. The basis of LED construction is formation of a p–n junction. Unintentionally doped ZnO usually presents n-type conductivity. It is difficult to obtain p-type ZnO of high quality because of its low dopant solubility, deep acceptor level, and self-compensation effect. Therefore, the initial ZnO LEDs were constructed with other p-type semiconductors to form p–n heterojunctions that exhibited electroluminescence (EL). In the early stages, ZnO light-emitting devices were mainly based on thin films. After the thin-film LEDs were realized, many researchers shifted their attention to the study of LEDs containing 1D ZnO nanomaterials.

In 2006, Chang and coworkers fabricated a heterojunction device consisting of a ZnO nanowire array on an n-GaN film on a sapphire substrate and the p-type polymer poly(3,4-ethylenedioxythiophene)/poly(styrenesulfonate) (PEDOT/PSS). This hybrid LED exhibited multiple EL peaks at forward bias, including ZnO band edge emission at about 383 nm and other peaks centered at 430, 640, and 748 nm [75]. Zhang et al. [76] synthesized an n-type ZnO nanowire array on a p-type GaN film by CVD to produce a hybrid LED with high brightness. UV–blue EL emission was observed from the heterojunction diode, which displayed a blue shift as the forward bias increased. Tang et al. [77] fabricated an LED based on single n-ZnO/p-AlGaIn heterojunction nanowires. A schematic illustration and SEM image of their LED are displayed in Figure 9a,b, respectively. When the injection current was 4 μ A, UV EL emission with a peak at 394 nm was observed, as shown in Figure 9c.

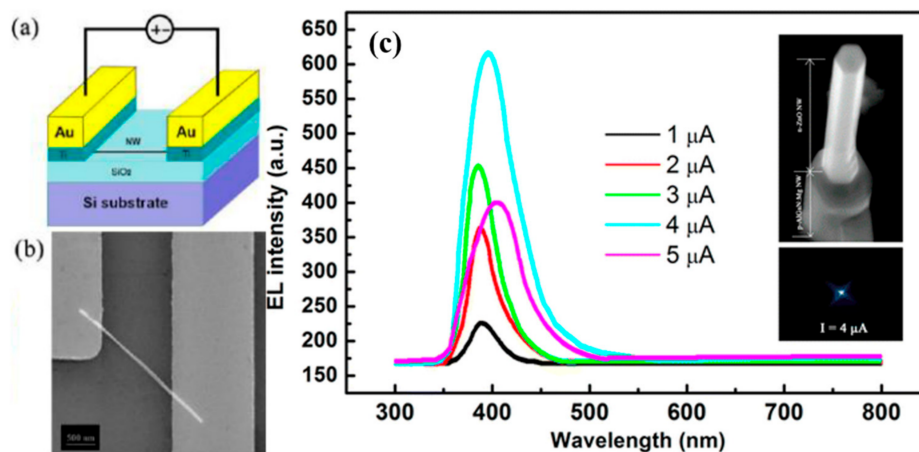


Figure 9. (a) Schematic illustration of the ZnO/AlGaIn heterojunction light-emitting diode (LED); (b) SEM image of a single ZnO nanowire embedded in Au/Ti electrode films; (c) electroluminescence (EL) spectra of the LED at different injection currents. Insets: (upper) SEM image of a single nanowire; (lower) CCD image of the LED at an injection current of 4 μA [77]. Reproduced with permission.

Heterojunction diodes have been fabricated using n-type ZnO nanomaterials and p-type organic/inorganic materials such as GaN [78–80], AlGaIn, Si [81,82], MgZnO [83], NiO [84], Cu₂O, SiC, *N,N'*-di(naphth-2-yl)-*N,N'*-diphenylbenzidine (NPB) [85], PEDOT/PSS [75], and [2-methoxy-5-(2-ethylhexyloxy)-1,4-phenylenevinylene] (MEH-PPV) [86]. Representative results for heterojunction LEDs containing 1D ZnO nanostructures, along with a brief description of the corresponding device structure, applied bias, and EL performance, are summarized in Table 1.

Table 1. 1D ZnO nanostructure-based heterojunction LEDs.

Device Structure	Turn-On Voltage	Threshold Voltage of Emission	Bias/Current	Wavelength of EL Peak	Ref.
ZnO nanowire arrays/P-GaN	3 V	4.4 V	5–7 V/0.5–1.5 mA	397 nm	[78]
ZnO nanowire arrays/P-GaN	3 V	4.4 V	6.5 V/2.6 mA	397 nm	[79]
n-GaN/ZnO nanorod/P-GaN	5 V		6 V	382 nm, 430 nm	[80]
Sb-doped p-ZnO nanowire arrays/n-GaN	3.74 V	4.0 V	16 V	391 nm	[87]
n-ZnO/p-AlGaIn	2 V		4 μA	394 nm	[77]
ITO/n-ZnO nanorod array/p+-Si	5 V (5 mA)	6 V	9.5 V/29.5 mA	450 nm, 700 nm	[81]
n-ZnO nanorod/p-Si			9.5 V	387 nm, 535 nm	[88]
p-Zn _{0.68} Mg _{0.32} O:N/n-ZnO nanowire	4.2 V		5 mA/125 mA cm ²	390 nm	[83]
p-NiO/n-ZnO nanowire	2.5 V	7 V	15 V	385 nm, 570 nm	[84]
ZnO nanowire/polymer (PEDOT/PSS)		<3 V	3 V	383, 430, 640, 748 nm	[75]
ZnO nanorod/NPB			22 mA/cm ²	342 nm	[85]
ZnO nanorods/MEH-PPV			28 V	380, 580, 615, 640, 747 nm,	[86]

Many research groups are committed to obtaining p-type ZnO materials and have observed EL emission from ZnO p–n homojunctions. To date, p-type ZnO nanostructures have been realized by doping ZnO with group-V elements, including N [89], P [74,90], As [91,92], and Sb [93]. However, there have been relatively few reports of p–n homojunction LEDs based on 1D ZnO nanostructures.

Sun and coworkers obtained p-ZnO by As ion implantation into as-grown ZnO nanorods and then constructed ZnO nanorod homojunction LEDs [92]. A schematic illustration of the homojunction LED

is presented in Figure 10a. At forward bias, UV emission originating from free-exciton recombination centered at about 380 nm was dominant, and a weak broad peak centered at about 630 nm was observed in EL spectra collected at room temperature. The second harmonic of UV emission centered at about 760 nm was also detected, as displayed in Figure 10b. The same group also used P as an acceptor dopant to fabricate ZnO nanorod homojunction LEDs by P ion implantation [74]. Strong UV emission attributed to near-band-edge emission and weak visible emission related to deep-level defects were observed from both devices at forward bias.

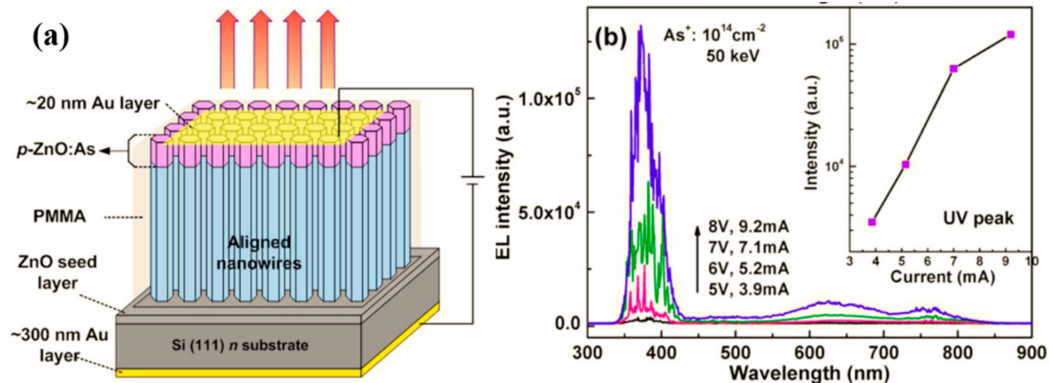


Figure 10. (a) Schematic illustration of an As-doped p-ZnO/n-ZnO nanorod homojunction LED; (b) EL spectra of a ZnO nanorod homojunction doped with As⁺ at 50 keV and 10^{14} cm^{-2} [92]. Reproduced with permission.

However, there are some problems associated with heterojunction and homojunction LEDs based on 1D ZnO nanostructures, which can prevent the development and application of ZnO-based LEDs. For example, the heterostructured devices suffer from p-ZnO doping and large lattice mismatch. A Schottky-type LED based on Au/ZnO nanowires was constructed to overcome these issues [94]. A schematic illustration of the LED is shown in Figure 11a. The EL spectra in Figure 11b reveal that the LED displayed excitonic EL emission at about 380 nm at high forward bias.

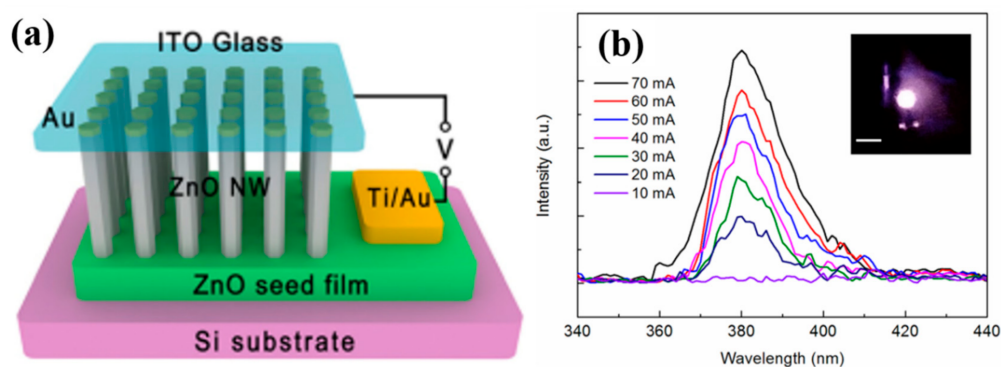


Figure 11. (a) Schematic illustration of the Au/ZnO nanowire Schottky LED; (b) EL spectra of the Schottky LED operating under different injection currents. Inset is a photograph of the device operating at an injection current of 70 mA [94]. Reproduced with permission.

Although there have been some encouraging achievements in LEDs based on 1D ZnO nanostructures, there are still some problems like the degradation of efficiency and stability caused by surface defects, surface adsorption, the low quality of p-type ZnO, and/or a high content of heterointerface defects. Surface passivation has been recognized as a promising approach to improve the EL performance of ZnO-based LEDs. In this approach, a dielectric/semiconductor material is coated on the surface of the 1D ZnO nanomaterial to form a core/shell nanostructure. Liu et al. [95]

fabricated two types of LEDs on p-GaN films using MgZnO-coated and bare ZnO nanorod arrays as active layers, as shown in Figure 12a. The EL performance of two types of LEDs is compared in Figure 12b. A strong emission peak at 387 nm was present in the EL spectra of both devices. The EL intensity of the MgZnO-coated LED was much higher than that of the uncoated one, which was attributed to the enhancement of the radiative recombination of the ZnO nanorods caused by the effective passivation of dangling bonds on the nanorod surface and the carrier confinement effect offered by the MgZnO coating. The stability of both devices exposed to ambient air for over a year at the same injection current of 5 mA was investigated at regular intervals; the results are displayed in Figure 12c. The ZnO near-band-edge UV emissions of both devices gradually decayed over time, but the decay rate of the uncoated device was faster than that of the MgZnO-coated LED. Therefore, the MgZnO-coated device exhibited higher stability than that of the uncoated one because surface adsorption on the nanorods was suppressed by the MgZnO coating. SiO₂ [96] and MgO [97] can also be used as passivation materials to improve the performance of 1D ZnO nanostructure LEDs.

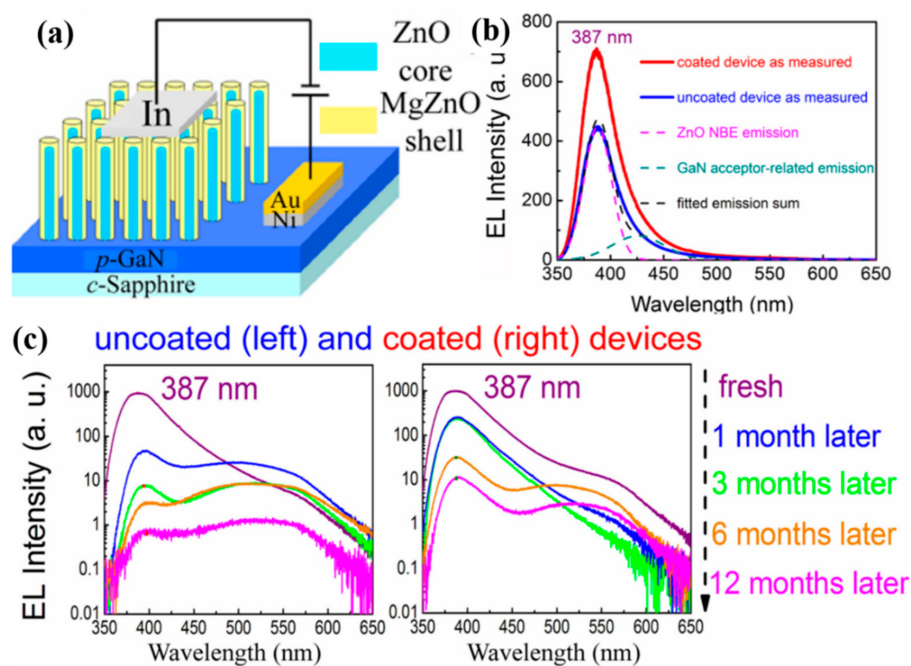


Figure 12. (a) Schematic illustration of an MgZnO-coated ZnO nanorod/p-GaN film LED; (b) EL spectra and Gaussian deconvolution analysis of the LEDs with and without an MgZnO coating under an injection current of 3.5 mA at room temperature; (c) EL spectra of LEDs with (right) and without (left) an MgZnO coating after exposure to air for different periods at an injection current of 5 mA [95]. Reproduced with permission.

Another effective approach to improve the luminous efficiency of LEDs is to introduce LSPs into the LED structure. Semiconductor excitons/photons can be resonantly coupled with the metal LSPs and then scattered/re-emitted into free space as radiation. This approach provides additional recombination/extraction pathways, which can increase the spontaneous radiation rate, internal quantum efficiency, and light extraction efficiency of the LEDs. Liu and coworkers fabricated ZnO nanorod array/p-GaN film heterostructure LEDs embedded in an Ag nanoparticle/polymethyl methacrylate (PMMA) composite [98]. A typical cross-sectional SEM image and schematic illustration of such an LED are shown in Figure 13a,b, respectively. The UV emission from ZnO excitons was enhanced more than 13-fold in EL spectra (Figure 13c). Lu et al. [99] constructed an Al nanoparticle-decorated n-ZnO nanorod/p-GaN film LED. They obtained 30-fold EL enhancement compared with that of the device without Al nanoparticles because of the effect of Al LSPs.

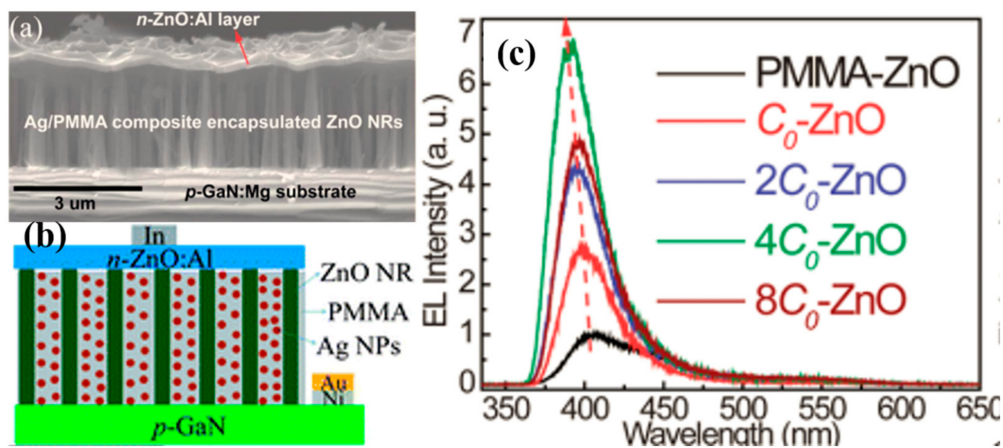


Figure 13. (a) Cross-sectional SEM image and (b) schematic illustration of a ZnO nanorod array/*p*-GaN film heterostructure LED embedded in a Ag nanoparticle/polymethyl methacrylate (PMMA) composite; (c) EL spectra of LEDs with different Ag nanoparticle concentrations in PMMA at an injection current of 5 mA at room temperature. $C_0 = 6.5 \times 10^{15} \text{ cm}^{-3}$ [98]. Reproduced with permission.

To further improve the performance of LEDs, the two methods mentioned above can be combined. Zhang et al. [100] fabricated LSP-enhanced waveguide-type UV LEDs via sputtering Ag nanoparticles onto ZnO/MgZnO core/shell nanorod array/*p*-GaN film heterostructures. After decoration with Ag nanoparticles, the UV emission intensity of the ZnO/MgZnO core/shell nanorod array showed a ~9-fold enhancement compared with that of the device without Ag nanoparticles because of coupling with LSPs. The next year, the same group constructed LSP-enhanced UV LEDs by spin-coating Ag nanoparticles on ZnO/SiO₂ core/shell nanorod array/*p*-GaN heterostructures; a schematic diagram of this LED structure is illustrated in Figure 14a [96]. The EL intensity was enhanced when both Ag nanoparticles and a SiO₂ spacer layer were coated on the surface of the ZnO nanorods, as shown in Figure 14b. The effect of the SiO₂ spacer-layer thickness on the UV emission intensity was investigated. A maximum EL enhancement of ~7-fold was obtained when the thickness of the SiO₂ spacer layer was 12 nm. In contrast, a maximum PL enhancement of ~3.5-fold was achieved when the SiO₂ spacer layer was 16 nm thick. The EL enhancement was attributed to the combined effects of internal quantum efficiency improvement caused by exciton–LSP coupling and extraction efficiency enhancement induced by photon–LSP coupling.

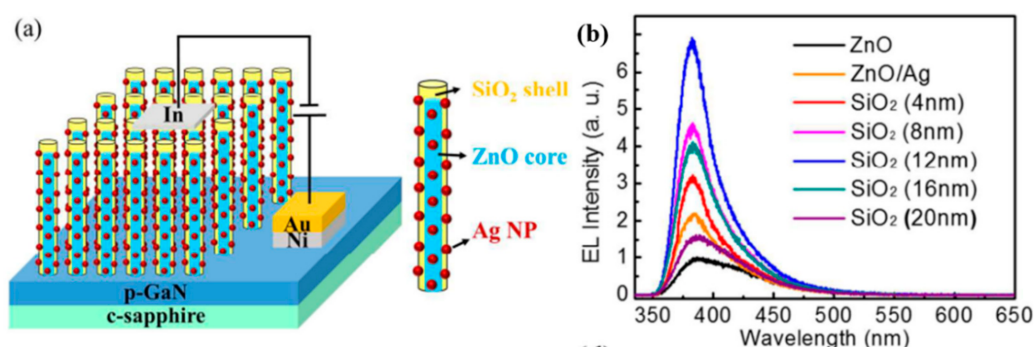


Figure 14. (a) Schematic diagram of a localized surface plasmon (LSP)-enhanced ZnO/SiO₂ core/shell nanorod array LED; (b) room-temperature EL spectra of bare and Ag-decorated ZnO core/shell nanorod arrays with different SiO₂ shell thicknesses under an injection current of 5 mA [96]. Reproduced with permission.

A near-UV LED based on a ZnO nanorod/MEH-PPV heterostructure using a ZnS layer as a buffer layer was reported by Wang and colleagues [101]. The intensity of near-UV EL was enhanced 10-fold compared with that of the device without a ZnS layer. In particular, the turn-on voltage was obviously decreased. In addition, the ZnS layer could induce recombination center of carriers, which regulated the EL wavelength of the heterojunction. Wei et al. [102] fabricated ZnO nanowire/p-GaN heterojunction LEDs containing ZnS particles to sensitize the ZnO nanowires. Localized states formed at the ZnO/ZnS interface, generating a built-in electric field, which captured electrons and holes at the ZnO/ZnS interface, where they recombined to result in EL emission from ZnO. Moreover, the piezo-phototronic effect can improve the efficiency of flexible ZnO nanowire/p-polymer hybridized LEDs [103,104]. Wang et al. [104] fabricated a hybrid LED based on a ZnO nanowire/p-polymer heterostructure. The external quantum efficiency of the hybrid LED at least doubled upon applying strain, reaching 5.92%.

4.2. Photodetectors

UV photodetectors are important photoelectric devices that occupy an indispensable position in today's information society. UV photodetectors are widely used in the military (e.g., UV control and guidance, UV alarms, and UV resistance), as well as in civil fields such as fire alarms, UV communication, ozone hole detection, and water purification. Therefore, the further development of UV detection technology has important implications in modern national defense and daily life. The importance and universality of UV photodetectors in military and civilian fields also make them a focus of current research.

ZnO has a wide direct band gap at room temperature of about 3.37 eV, along with high chemical and thermal stability, strong ability to resist radiation damage, and low content of electron-induced defects. Because of these favorable features, ZnO is widely used in UV detectors. Early ZnO UV detectors were mainly based on membrane structures [105]. However, with the development of low-dimensional materials, photodetectors based on 1D nanomaterials have attracted interest. Compared with UV detectors based on thin films and bulk materials, those based on 1D ZnO nanostructures display higher responsivity and internal photoconductive gain. This is because 1D nanomaterials have a large surface-to-volume ratio and the presence of deep-level surface trap states can prolong the lifetime of photogenerated electrons and holes. In addition, the low dimensionality of the active area can shorten the transit time of carriers [4,106]. There are several types of photodetector structures, such as photoconductive, metal–semiconductor–metal (MSM), Schottky [107], and p–n junction [108–110] photodetectors.

In 2002, Yang and coworkers first detected the UV response of an individual ZnO nanowire [111]. The conductance of a single ZnO nanowire was very sensitive to UV light. The resistivity of a ZnO nanowire reversibly changed by 4–6 orders of magnitude under UV illumination. In 2007, Soci et al. [4] reported a UV photodetector based on a single ZnO nanowire with an internal photoconductive gain as high as $\sim 10^8$. While the photoconductive detector showed slow response times because of possible persistent photoconductivity effects, it usually worked with an external power source.

To realize ZnO-based UV photodetectors with high sensitivity and fast response time, a Schottky contact instead of an ohmic contact was adopted [107,112–115]. For example, Zhou and coworkers fabricated a Schottky junction-type photodetector that used ZnO nanowire and Pt metal electrode to form Schottky contact [98]. The UV sensitivity of the photodetector was enhanced by $\sim 10^4$, and its recovery time was markedly shortened from ~ 417 to ~ 0.8 s, as shown in Figure 15.

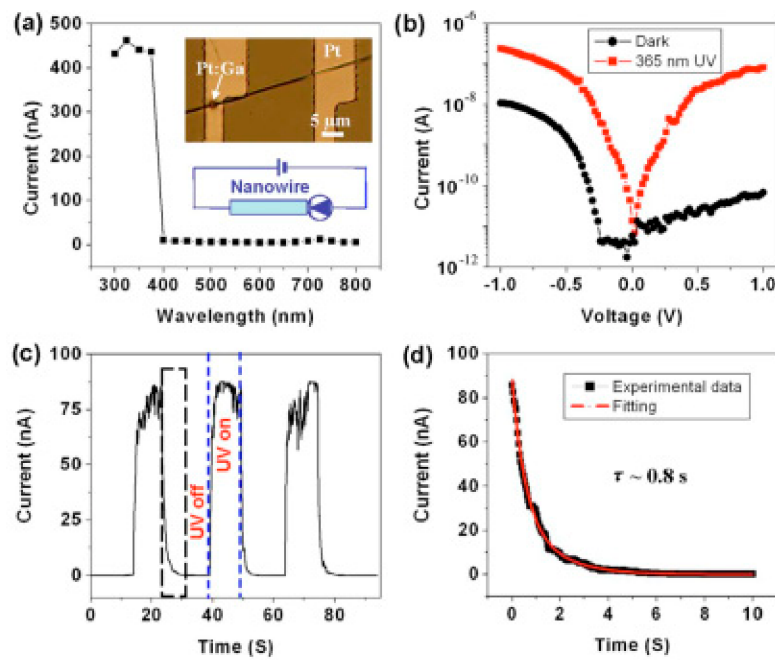


Figure 15. (a) The current of a ZnO nanowire UV detector as a function of the wavelength of incident light. Insets are an optical microscope image (upper) and schematic structure (lower) of the Schottky-type ZnO nanowire device; (b) current–voltage characteristics of the photodetector in the dark and under 365 nm UV illumination; (c) time dependence of the device photocurrent under on/off switching of 365 nm UV illumination (the applied bias was 1 V); (d) experimental data points and fitting curve of the photocurrent decay [113]. Reproduced with permission.

Nie and coworkers [115] reported a Schottky junction UV photodetector based on transparent monolayer graphene (MLG)/ZnO nanorods. The photodetector showed a ratio of photocurrent to dark current of approximately 3 orders of magnitude under 365 nm UV illumination at a bias of -1 V. The responsivity and photoconductive gain of the detector were 113 A W^{-1} and 385, respectively (Figure 16). The response speed of the UV photodetector was rather fast, with rise and fall times of 0.7 and 3.6 ms, respectively, which was attributed to the formation of a Schottky barrier, high crystal quality of the ZnO nanorod array, and strong light-trapping effect of the structure.

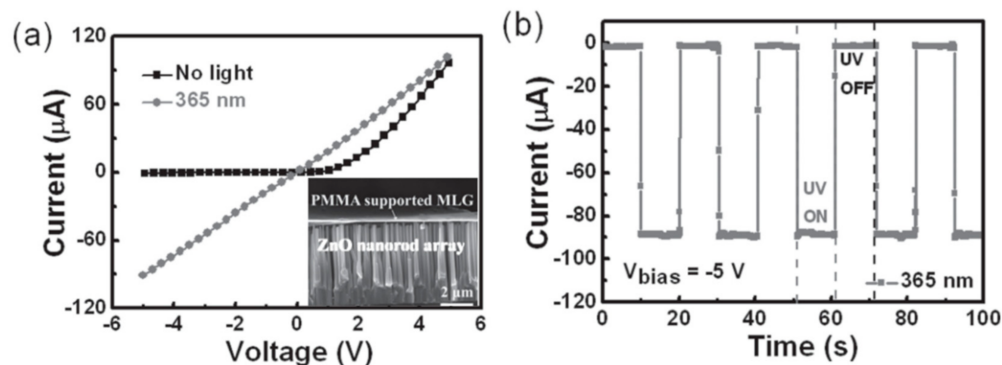


Figure 16. (a) Current–voltage characteristics of the monolayer graphene (MLG)/ZnO nanorod UV photodetector in the dark and under 365 nm UV illumination with an incident intensity of $100 \mu\text{W cm}^{-2}$. Inset is a cross-sectional SEM image of the PMMA-supported MLG film/ZnO nanorod Schottky photodetector; (b) response times of the MLG/ZnO nanorod UV photodetector. The applied bias was -1 V [115]. Reproduced with permission.

Several kinds of 1D ZnO nanostructure-based p–n junction photodetectors have been reported [108,110,116,117], which possess the advantages of low applied fields and no oxygen dependency over Schottky junction detectors. In particular, p–n junction photodetectors work at rather high bias voltage to inhibit the recombination of electron–hole pairs, which increases the detection capability of UV signals [108,118]. Tahani et al. [108] developed a photodetector based on p-Si/n-ZnO nanotube heterojunctions, which is shown in Figure 17. Under 365 nm UV illumination with an incident power intensity of 1 mW cm^{-2} at a bias of -2 V , the responsivity and detectivity of the detector were 21.51 A W^{-1} and $1.26 \times 10^{12} \text{ cm Hz}^{1/2} \text{ W}^{-1}$, along with an external quantum efficiency of $73.1 \times 10^2\%$ (effective area = $\sim 0.79 \text{ mm}^2$). The rise and fall times of the heterojunction device were 0.44 and 0.599 s, respectively.

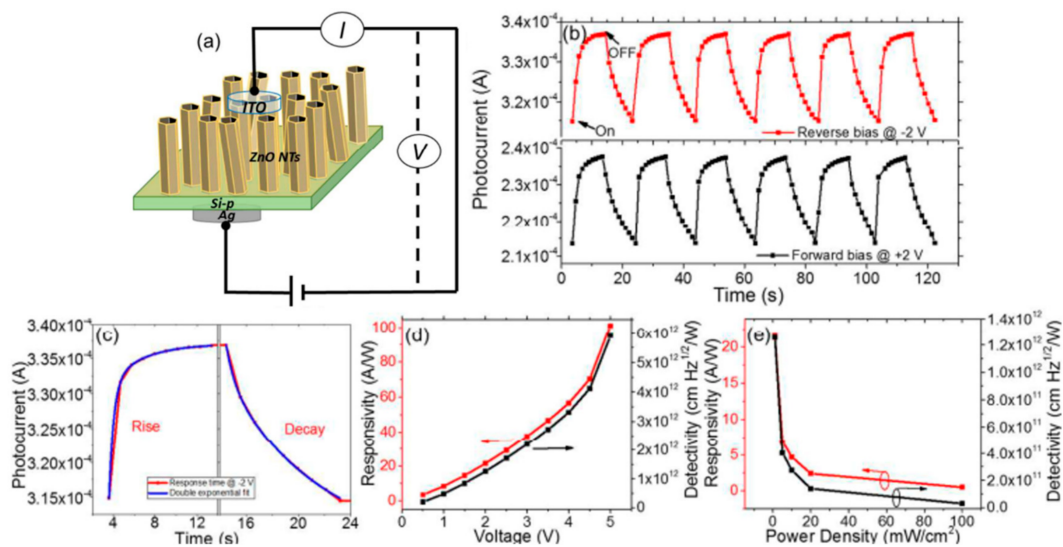


Figure 17. (a) Schematic diagram of the structure of a p-Si/n-ZnO nanotube UV photodetector; (b) detector photoresponse under 365 nm UV illumination with an incident intensity of 1 mW cm^{-2} at a bias of $\pm 2 \text{ V}$; (c) response times of the photodetector under 365 nm illumination (1 mW cm^{-2}) at a bias of -2 V ; (d) device responsivity and detectivity as functions of applied bias under 365 nm illumination (1 mW cm^{-2}); (e) responsivity and detectivity as functions of light intensity under 365 nm illumination at a bias of -2 V [108]. Reproduced with permission.

Recently, self-powered ZnO photodetectors have attracted research interest because they can work in some poor conditions without an external power source. According to their interface features, self-powered photodetectors have three types of structures: Schottky junction, p–n junction, and photoelectrochemical. Compared with the other two types, ZnO-based p–n junction UV detectors are more suitable for development as self-powered photodetectors because of their much lower applied fields, faster response times, and high stability. Table 2 summarizes representative results for reported 1D ZnO nanostructure-based self-powered UV photodetectors, accompanied with a brief description of the corresponding device characteristics, detection wavelengths, power intensity, and photodetector performance.

Table 2. Recently reported self-powered 1D ZnO nanostructure-based UV photodetectors.

Device Structure	Light of Detection, Power	UV-Visible Rejection Ratio	On/Off Ratio	Responsivity	Rise/Decay Time	Ref.
ZnO/Sb-doped ZnO nanowire	365 nm, 0.3 mW cm^{-2}		26.7	26.5	30 ms/30 ms	[119]
n-ZnO nanowire/P-GaN film					20 μs /219 μs	[120]

Table 2. Cont.

Device Structure	Light of Detection, Power	UV-Visible Rejection Ratio	On/Off Ratio	Responsivity	Rise/Decay Time	Ref.
n-ZnO nanorods/i-MgO/p-GaN	350 nm	R350 nm/R500 nm) = 34.5	8000	0.32 A/W		[121]
ZnO nanorods/Si				UV/Visible: 0.3 A W ⁻¹ /0.5 A W ⁻¹		[122]
ZnO Nanowire/CuSCN	370 nm, 100 mW/cm ²	R370 nm/R500 nm) = 100		0.02 A/W		[123]
ZnO Nanorod/CuSCN	380 nm	100		0.0075 A W ⁻¹	5 ns/6.7 us	
PEDOT:PSS/ZnO micro-/nanowire			1000			[124]
n-ZnO/p-NiO core-shell nanowire				0.493 mA W ⁻¹	1.38 ms/10.0 ms and 30.3 ms	[125]
p-NiO/n-ZnO nanorod array	355 nm			0.44 mA W ⁻¹	0.23 s/0.21 s	[126]
p-NiO/n-ZnO nanowire	380 nm, 0.36 mW/cm ²			1.4 mA/W		[127]
CH ₃ NH ₃ PbI ₃ perovskite/ZnO nanorod				3.9 A W ⁻¹ 300 nm	0.3 s/0.7 s	[128]
ZnO/Cu ₂ O nanowire						[129]

Various approaches have been adopted to improve the photoresponse performance of 1D ZnO nanostructure photodetectors for use in practical applications. Generally, surface and interface carrier transport modulation are the main routes used to raise photoresponsivity [130]. For instance, Lao et al. [131] manipulated and functionalized the polymer polystyrene sulfate (PSS) on the surface of ZnO nanobelts using a layer-by-layer self-assembly method. The sensitivity of the PSS-coated ZnO nanobelt-based detector was improved by close to 5 orders of magnitude compared with that of the device lacking PSS, which was ascribed to the energy levels introduced by PSS serving as a “hopping” state or bridge for electron transfer, effectively increasing the excitation probability of an electron to the conduction band.

In addition, functional devices consisting of a noble metal (e.g., Au [132,133] and Ag [134–137]) coated on semiconductor nanostructures have inspired extensive research effort. Such devices can realize superior optoelectronic properties to those without a metal coating because their LSPR effect leads to strong scattering and absorption of incident light, efficient separation of photogenerated electron–hole pairs, and rapid transport of charge carriers at the metal/semiconductor interface. Liu and coworkers fabricated ZnO nanowire photodetectors coated with Au nanoparticles [132]. The ratio of photocurrent to dark current of the ZnO photodetector with Au nanoparticles reached up to 5×10^6 , which was much larger than that of the device without Au nanoparticles (around 10^3). Moreover, the decay time of the device decreased from ~ 300 s to ~ 10 s after coating with Au nanoparticles.

Al is an abundant and inexpensive metal that is a better plasmonic material than Au and Ag in the UV range because of the negative real part and relatively low imaginary part of its dielectric function [138]. Lu et al. [139] used LSP resonance mediated by Al nanoparticles to optimize the UV response of a ZnO nanorod array photodetector. The responsivity of the photodetector was improved from 0.12 to 1.59 A W⁻¹ after modification with Al nanoparticles and the ratio of photocurrent to dark current was enhanced 6-fold compared with that of the bare one, as displayed in Figure 18. Furthermore, the rise and decay times of the photodetector decreased from 0.8 and 0.85 s, respectively, to less than 0.03 and 0.035 s, respectively, after Al nanoparticle decoration.

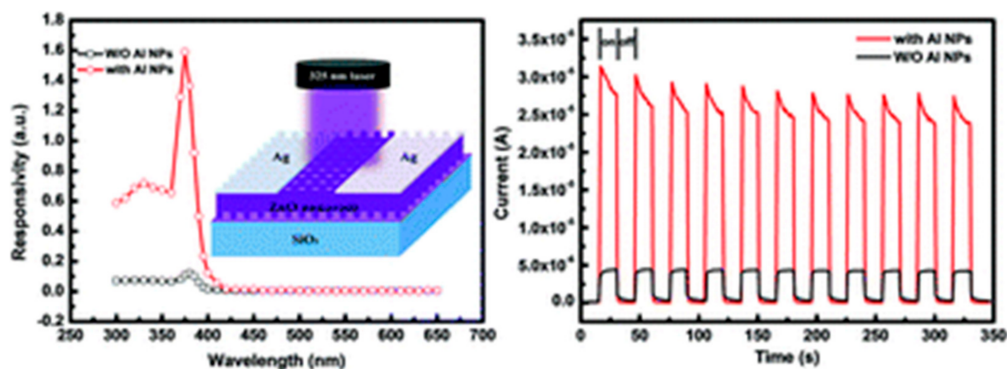


Figure 18. (a) Photoresponsivity spectra of ZnO nanorod photodetectors without and with Al nanoparticles. Inset is a schematic of the device structure; (b) time response of the devices with and without Al nanoparticles under 325 nm illumination at a bias of 5.0 V [139]. Reproduced with permission.

The transition metal Co is an effective candidate material for the surface modification of photodetectors. Buddha and coworkers fabricated a UV photodetector based on a Co-coated ZnO (Co-ZnO) nanorod array [140]; a schematic of the device is displayed in Figure 19a. The presence of defect states in the Co-ZnO nanorod detector raised the photocurrent compared with that of the device with bare ZnO nanorods. The Co-ZnO nanorod photodetector was sensitive to an external magnetic field; its response current increased by about 186% under an applied magnetic field of 2400 G compared with that without an applied magnetic field at the same bias voltage (Figure 19b). Furthermore, the response and recovery times of the photodetector decreased from 38 and 195 s, respectively, to less than 1.2 and 7.4 s, respectively, upon Co decoration, as shown in Figure 19c,d.

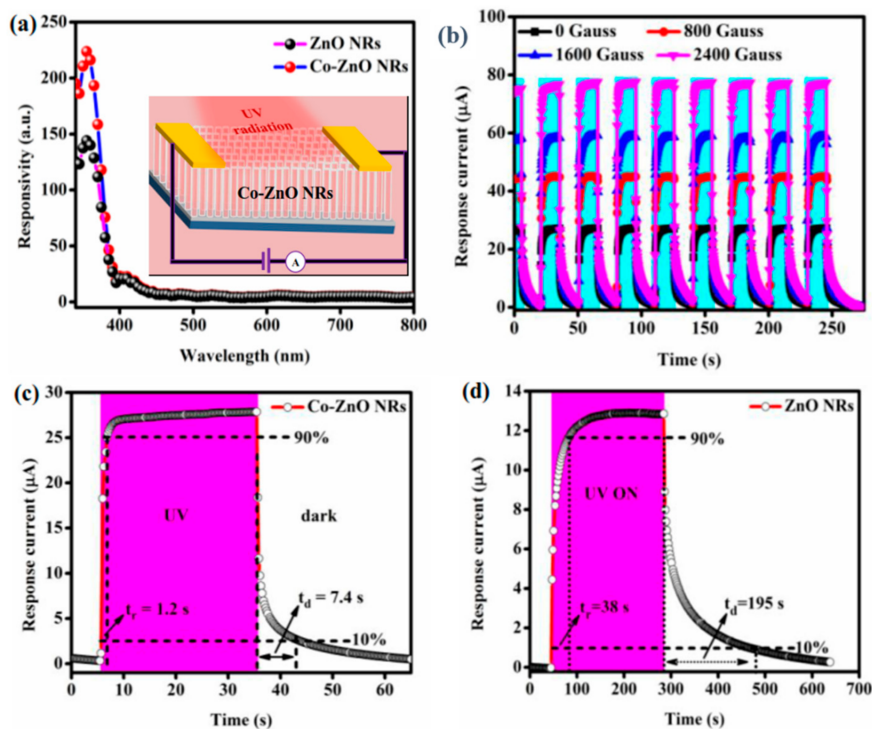


Figure 19. (a) Photoresponse spectra of photodetectors based on bare and Co-coated ZnO nanorods. The inset shows a schematic of the device; (b) cyclic response of the Co-coated ZnO nanorod photodetector with and without an external magnetic field at an applied bias of 5 V. The recovery times of (c) Co-coated and (d) bare ZnO nanorod photodetectors [140]. Reproduced with permission.

Recently, many researchers have attempted to improve the performance of photodetectors based on ZnO 1D nanostructures through the piezo-phototronic effect [141–146] and obtained some noticeable achievements. ZnO with a non-centrosymmetric crystal structure possesses high polarization. Therefore, the generation, transport, separation, and recombination process of carriers can be controlled by the piezopotential caused by the strain in this piezoelectric semiconductor material. It is worth noting that the coupled piezoelectric polarization, optoelectronic, and semiconducting properties of 1D ZnO nanomaterials offer an opportunity to construct functional devices with improved optoelectronic performance. Wang et al. [146] demonstrated that the responsivity of an MSM ZnO micro-/nanowire photodetector was enhanced through the piezoelectric effect. Zhang et al. [143] fabricated a self-powered photodetector based on a metal–insulator–semiconductor (MIS) Pt/Al₂O₃/ZnO structure; a schematic diagram of the device is shown in Figure 20a. The Schottky barrier height (SBH) was markedly enhanced to 0.739 eV by introducing the ultrathin dielectric layer (Al₂O₃) at the interface. The SBH could be actively adjusted by the modulation of the piezopolarization-induced built-in electric field under compressive strain, as shown in Figure 20b. The responsivity and detectivity of the photodetector increased from 0.644 $\mu\text{A W}^{-1}$ and $2.92 \times 10^6 \text{ cm Hz}^{0.5} \text{ W}^{-1}$, respectively, without compressive strain to 0.644 $\mu\text{A W}^{-1}$ and $2.92 \times 10^6 \text{ cm Hz}^{0.5} \text{ W}^{-1}$, respectively, under compressive strain of -1.0% .

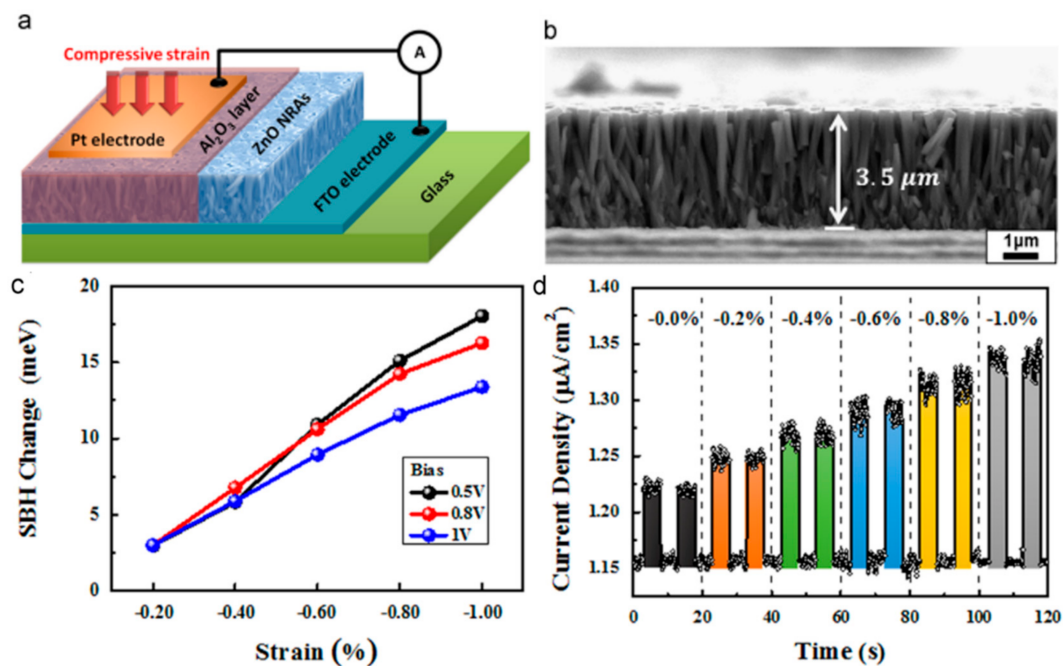


Figure 20. (a) Schematic diagram of the Pt/Al₂O₃/ZnO nanorod metal–insulator–semiconductor (MIS) photodetector; (b) typical cross-sectional SEM image of the ZnO nanorod array; (c) calculated Schottky barrier height (SBH) change under compressive strain at different biases of 0.5, 0.8, and 1 V; (d) device photoresponses under 100 mW cm^{-2} illumination and different compressive strains [143]. Reproduced with permission.

5. Conclusions

In conclusion, low-dimensional ZnO nanomaterials could be suitable for use in advanced optoelectronic devices, such as LEDs and photodetectors, because of their favorable properties. This review focused on the fabrication methods and growth parameters that influence the properties of the obtained 1D ZnO nanostructures. The fabricated nanomaterials could be used to construct novel devices with improved performance for certain applications. The properties, preparation, and device applications of 1D ZnO nanostructures were reviewed in detail. Importantly, several

promising approaches to improve device performance, including surface passivation, LSPs, and piezo-phototronic effects, were discussed.

Considering the wide application potential of 1D ZnO nanomaterials and their excellent performance in devices, they can satisfy the requirements of “smaller, faster, colder” for electronics, which is expected to be extended to practical applications in the near future. The applications of 1D ZnO nanomaterials have expanded greatly in recent years, and the performance of various devices has been continuously improved. Novel high-performance devices based on 1D ZnO nanomaterials will certainly be an important research focus of the nanotechnology industry in the 21st century. With the improvement of preparation technology, deepening of research, constant improvement of device performance, and progress of nanotechnology industrialization, 1D ZnO nanomaterials will play an increasingly important role in the fields of energy, environmental protection, information science technology, biomedicine, security, and national defense.

The fundamental properties and applications of 1D ZnO nanomaterials have been explored extensively to optimize their advantages, providing a route to meet practical requirements in nanoscience and nanotechnology. Because 1D ZnO nanomaterials possess a large binding exciton energy, wide band gap, high carrier mobility, and non-centrosymmetric structure, they can be used to couple different properties such as semiconductivity, piezoelectricity, and photoexcitation together to develop next-generation devices with attractive properties such as intelligent features and high efficiency. At present, much attention has been paid to LEDs and photodetectors based on 1D ZnO nanomaterials, and more and more interdisciplinary research has been conducted, such as biochemical applications of 1D ZnO nanomaterials. It is anticipated that the carrier transport in 1D ZnO nanomaterials can be well tuned to maximize conversion efficiency. Through the combination of semiconducting properties and piezo-phototronic and size effects, the energy band structure of devices could be tuned to modulate charge carrier transport behavior, and device performance could be improved by controlling the SBH. Therefore, coupled effects can be readily applied to 1D ZnO nanomaterial-based devices to improve performance. We anticipate that research on 1D ZnO nanomaterial-based optoelectronic devices, such as LEDs and photodetectors, will yield further progress.

6. Perspective

There has been extensive and fundamental research performed on 1D ZnO nanomaterials and devices, resulting in methods to construct intelligent, smart, functional units with advanced performances for potential applications. One-dimensional ZnO nanomaterials generally have non-central symmetry crystal structure, high crystal quality, large aspect ratio, high carrier mobility, wide band gap, and other characteristics that can be applied for coupling with properties such as photoexcitation, piezoelectricity, and semiconductivity for designing next-generation, newly emerging devices. At present, many types of 1D ZnO nanodevices have emerged with promising applications, for example, energy harvesting, piezo-phototronic light emitting, photodetecting, nano-biosensing, and so on, based on 1D ZnO nanomaterials. When considering the design factors for building several kinds of nanodevices based on 1D ZnO nanomaterial, charge carrier generation, transport, and recombination dynamics are generally considered by studying band gap structure, non-central symmetry induced piezotronic effects, surface or interface contact properties, and so on. Thus, conversion efficiency could be key in the overall consideration for building advanced optoelectric devices with improved performance. Until now, it was anticipated that the charge carrier transport behaviors of the 1D ZnO nanomaterials could be well modulated for building devices based on piezotronic and piezo-phototronic effects. Self-powered 1D ZnO nanodevices could be constructed with outperforming properties based on the above effects, thus, next-generation, intelligent products with smart volume could be built by applying the mentioned ideas. By optimally combining their properties based on 1D ZnO nanomaterials, the performance of these devices, such as nanogenerators, LEDs, photodetectors, nanosensors, and memory devices, can be improved by modulating charge carrier transport behavior,

interface barrier structures, piezotronic effect, and so on. It is believed that the coupled effects can be well applied for modulating carrier transport behaviors in 1D ZnO nanodevices for improving their performance. Further, newly emerging 1D ZnO nanodevices could be constructed for promising applications by studying its known effects and other properties through doping and surface modification. Finally, we anticipate that research work on 1D ZnO nanodevices—such as LEDs, photodetectors, solar cells, nanosensors, nanogenerators, and others—will yield continuous progress, and novel optoelectric, light emitting, electric nanodevices could be created through further efforts.

Author Contributions: The manuscript was written through contributions of all authors. All authors have given approval to the final version of the manuscript.

Acknowledgments: This work was supported by the National Natural Science Foundation of China (Grant Nos. 61504048, 51675517, and 61505241), Natural Science Fund of Jiangsu Province (Grant Nos. BK20140380 and BK20160057), Youth Innovation Promotion Association Chinese Academy of Sciences (Grant No. 2014280), Ministry of Science and Technology focused on Special International Cooperation Projects (Grant No. 2016YFE0107700), Jiangsu Planned Projects for Postdoctoral Research Funds (Grant No. 1701010A), Major Technology Innovation Projects of Jiangsu Province (Grant No. BO2015007), China Postdoctoral Science Foundation (Grant No. 2016M601890), Shenzhen Key Laboratory Project (Grant No. ZDSYS201603311644527), Shenzhen Fundamental Research Fund (Grant Nos. JCYJ20150611092848134 and JCYJ20150929170644623), and the Shenzhen Science and Technology Innovation Fund (Grant No. KQCX20140522143114399).

Conflicts of Interest: The authors declare no conflict of interest.

References

1. Wang, Z.L. Zinc oxide nanostructures: Growth, properties and applications. *J. Phys. Condens. Matter* **2004**, *16*, R829–R858. [[CrossRef](#)]
2. Vayssieres, L. Growth of arrayed nanorods and nanowires of ZnO from aqueous solutions. *Adv. Mater.* **2003**, *15*, 464–466. [[CrossRef](#)]
3. Greene, L.E.; Law, M.; Tan, D.H.; Montano, M.; Goldberger, J.; Somorjai, G.; Yang, P. General route to vertical ZnO nanowire arrays using textured ZnO seeds. *Nano Lett.* **2005**, *5*, 1231–1236. [[CrossRef](#)] [[PubMed](#)]
4. Soci, C.; Zhang, A.; Xiang, B.; Dayeh, S.A.; Aplin, D.P.R.; Park, J.; Bao, X.Y.; Lo, Y.H.; Wang, D. ZnO Nanowire UV Photodetectors with High Internal Gain. *Nano Lett.* **2007**, *7*, 1003–1009. [[CrossRef](#)] [[PubMed](#)]
5. Huang, M.H.; Wu, Y.; Feick, H.; Tran, N.; Weber, E.; Yang, P. Catalytic Growth of Zinc Oxide Nanowires by Vapor Transport. *Adv. Mater.* **2001**, *13*, 113–116. [[CrossRef](#)]
6. Fang, F.; Zhao, D.X.; Zhang, J.Y.; Shen, D.Z.; Lu, Y.M.; Fan, X.W.; Li, B.H.; Wang, X.H. Growth of well-aligned ZnO nanowire arrays on Si substrate. *Nanotechnology* **2007**, *18*, 235604. [[CrossRef](#)]
7. Jung, S.H.; Oh, E.; Lee, K.H.; Park, W.; Jeong, S.H. A Sonochemical Method for Fabricating Aligned ZnO Nanorods. *Adv. Mater.* **2007**, *19*, 749–753. [[CrossRef](#)]
8. Kim, K.S.; Jeong, H.; Jeong, M.S.; Jung, G.Y. Polymer-Templated Hydrothermal Growth of Vertically Aligned Single-Crystal ZnO Nanorods and Morphological Transformations Using Structural Polarity. *Adv. Funct. Mater.* **2010**, *20*, 3055–3063. [[CrossRef](#)]
9. Liu, B.; Zeng, H.C. Hydrothermal Synthesis of ZnO Nanorods in the Diameter Regime of 50 nm. *J. Am. Chem. Soc.* **2003**, *125*, 4430–4431. [[CrossRef](#)] [[PubMed](#)]
10. Wang, W.Z.; Zeng, B.Q.; Yang, J.; Poudel, B.; Huang, J.Y.; Naughton, M.J.; Ren, Z.F. Aligned Ultralong ZnO Nanobelts and Their Enhanced Field Emission. *Adv. Mater.* **2006**, *18*, 3275–3278. [[CrossRef](#)]
11. Lu, C.; Qi, L.; Yang, J.; Tang, L.; Zhang, D.; Ma, J. Hydrothermal growth of large-scale micropatterned arrays of ultralong ZnO nanowires and nanobelts on zinc substrate. *Chem. Commun.* **2006**, *0*, 3551–3553. [[CrossRef](#)] [[PubMed](#)]
12. Yang, J.; Liu, G.; Lu, J.; Qiu, Y.; Yang, S. Electrochemical route to the synthesis of ultrathin ZnO nanorod/nanobelt arrays on zinc substrate. *Appl. Phys. Lett.* **2007**, *90*, 103109. [[CrossRef](#)]
13. Wang, X.; Ding, Y.; Summers, C.J.; Wang, Z.L. Large-Scale Synthesis of Six-Nanometer-Wide ZnO Nanobelts. *J. Phys. Chem. B* **2004**, *108*, 8773–8777. [[CrossRef](#)]
14. Sun, Y.; Fuge, G.M.; Fox, N.A.; Riley, D.J.; Ashfold, M.N.R. Synthesis of Aligned Arrays of Ultrathin ZnO Nanotubes on a Si Wafer Coated with a Thin ZnO Film. *Adv. Mater.* **2005**, *17*, 2477–2481. [[CrossRef](#)]

15. Xing, Y.J.; Xi, Z.H.; Xue, Z.Q.; Zhang, X.D.; Song, J.H.; Wang, R.M.; Xu, J.; Song, Y.; Zhang, S.L.; Yu, D.P. Optical properties of the ZnO nanotubes synthesized via vapor phase growth. *Appl. Phys. Lett.* **2003**, *83*, 1689–1691. [[CrossRef](#)]
16. Wei, A.; Sun, X.W.; Xu, C.X.; Dong, Z.L.; Yu, M.B.; Huang, W. Stable field emission from hydrothermally grown ZnO nanotubes. *Appl. Phys. Lett.* **2006**, *88*, 213102. [[CrossRef](#)]
17. Reimer, T.; Paulowicz, I.; Röder, R.; Kaps, S.; Lupan, O.; Chemnitz, S.; Benecke, W.; Ronning, C.; Adelung, R.; Mishra, Y.K. Single Step Integration of ZnO Nano- and Microneedles in Si Trenches by Novel Flame Transport Approach: Whispering Gallery Modes and Photocatalytic Properties. *ACS Appl. Mater. Interfaces* **2014**, *6*, 7806–7815. [[CrossRef](#)] [[PubMed](#)]
18. Kaps, S.; Bhowmick, S.; Gröttrup, J.; Hrkac, V.; Stauffer, D.; Guo, H.; Warren, O.L.; Adam, J.; Kienle, L.; Minor, A.M.; et al. Piezoresistive Response of Quasi-One-Dimensional ZnO Nanowires Using an in Situ Electromechanical Device. *ACS Omega* **2017**, *2*, 2985–2993. [[CrossRef](#)]
19. Zhang, C.; Zhu, F.; Xu, H.; Liu, W.; Yang, L.; Wang, Z.; Ma, J.; Kang, Z.; Liu, Y. Significant improvement of near-UV electroluminescence from ZnO quantum dot LEDs via coupling with carbon nanodot surface plasmons. *Nanoscale* **2017**, *9*, 14592–14601. [[CrossRef](#)] [[PubMed](#)]
20. Mishra, Y.K.; Modi, G.; Cretu, V.; Postica, V.; Lupan, O.; Reimer, T.; Paulowicz, I.; Hrkac, V.; Benecke, W.; Kienle, L.; et al. Direct Growth of Freestanding ZnO Tetrapod Networks for Multifunctional Applications in Photocatalysis, UV Photodetection, and Gas Sensing. *ACS Appl. Mater. Interfaces* **2015**, *7*, 14303–14316. [[CrossRef](#)] [[PubMed](#)]
21. Özgür, Ü.; Alivov, Y.I.; Liu, C.; Teke, A.; Reshchikov, M.A.; Doğan, S.; Avrutin, V.; Cho, S.-J.; Morkoç, H. A comprehensive review of ZnO materials and devices. *J. Appl. Phys.* **2005**, *98*, 41301. [[CrossRef](#)]
22. Teng, M.; Min, G.; Mei, Z.; Yanjun, Z.; Xidong, W. Density-controlled hydrothermal growth of well-aligned ZnO nanorod arrays. *Nanotechnology* **2007**, *18*, 35605. [[CrossRef](#)]
23. Li, L.; Pan, S.; Dou, X.; Zhu, Y.; Huang, X.; Yang, Y.; Li, G.; Zhang, L. Direct Electrodeposition of ZnO Nanotube Arrays in Anodic Alumina Membranes. *J. Phys. Chem. C* **2007**, *111*, 7288–7291. [[CrossRef](#)]
24. Wang, Z.; Liu, X.; Gong, J.; Huang, H.; Gu, S.; Yang, S. Epitaxial Growth of ZnO Nanowires on ZnS Nanobelts by Metal Organic Chemical Vapor Deposition. *Cryst. Growth Des.* **2008**, *8*, 3911–3913. [[CrossRef](#)]
25. Woong, L.; Min-Chang, J.; Jae-Min, M. Fabrication and application potential of ZnO nanowires grown on GaAs(002) substrates by metal-organic chemical vapour deposition. *Nanotechnology* **2004**, *15*, 254. [[CrossRef](#)]
26. Heo, Y.W.; Varadarajan, V.; Kaufman, M.; Kim, K.; Norton, D.P.; Ren, F.; Fleming, P.H. Site-specific growth of ZnO nanorods using catalysis-driven molecular-beam epitaxy. *Appl. Phys. Lett.* **2002**, *81*, 3046–3048. [[CrossRef](#)]
27. Cao, B.Q.; Lorenz, M.; Rahm, A.; Wenckstern, H.v.; Czekalla, C.; Lenzner, J.; Benndorf, G.; Grundmann, M. Phosphorus acceptor doped ZnO nanowires prepared by pulsed-laser deposition. *Nanotechnology* **2007**, *18*, 455707. [[CrossRef](#)]
28. Acuña, K.; Yáñez, J.; Ranganathan, S.; Ramírez, E.; Pablo Cuevas, J.; Mansilla, H.D.; Santander, P. Photocatalytic degradation of roxarsone by using synthesized ZnO nanoplates. *Sol. Energy* **2017**, *157*, 335–341. [[CrossRef](#)]
29. Xu, F.; Shen, Y.; Sun, L.; Zeng, H.; Lu, Y. Enhanced photocatalytic activity of hierarchical ZnO nanoplate-nanowire architecture as environmentally safe and facilely recyclable photocatalyst. *Nanoscale* **2011**, *3*, 5020–5025. [[CrossRef](#)]
30. Song, J.; Kulinich, S.A.; Yan, J.; Li, Z.; He, J.; Kan, C.; Zeng, H. Epitaxial ZnO Nanowire-on-Nanoplate Structures as Efficient and Transferable Field Emitters. *Adv. Mater.* **2013**, *25*, 5750–5755. [[CrossRef](#)] [[PubMed](#)]
31. Weng, B.; Yang, M.-Q.; Zhang, N.; Xu, Y.-J. Toward the enhanced photoactivity and photostability of ZnO nanospheres via intimate surface coating with reduced graphene oxide. *J. Mater. Chem. A* **2014**, *2*, 9380–9389. [[CrossRef](#)]
32. Qiu, Y.; Yang, D.C.; Yin, B.; Lei, J.X.; Zhang, H.Q.; Zhang, Z.; Chen, H.; Li, Y.P.; Bian, J.M.; Liu, Y.H.; et al. Branched ZnO nanotrees on flexible fiber-paper substrates for self-powered energy-harvesting systems. *RSC Adv.* **2015**, *5*, 5941–5945. [[CrossRef](#)]
33. Cheng, L.; Chang, Q.; Chang, Y.; Zhang, N.; Tao, C.; Wang, Z.; Fan, X. Hierarchical forest-like photoelectrodes with ZnO nanoleaves on a metal dendrite array. *J. Mater. Chem. A* **2016**, *4*, 9816–9821. [[CrossRef](#)]

34. Jebril, S.; Kuhlmann, H.; Müller, S.; Ronning, C.; Kienle, L.; Duppel, V.; Mishra, Y.K.; Adelung, R. Epitactically Interpenetrated High Quality ZnO Nanostructured Junctions on Microchips Grown by the Vapor–Liquid–Solid Method. *Cryst. Growth Des.* **2010**, *10*, 2842–2846. [[CrossRef](#)]
35. Mishra, Y.K.; Adelung, R. ZnO tetrapod materials for functional applications. *Mater. Today* **2017**. [[CrossRef](#)]
36. Hrkac, S.B.; Koops, C.T.; Abes, M.; Krywka, C.; Müller, M.; Burghammer, M.; Sztucki, M.; Dane, T.; Kaps, S.; Mishra, Y.K.; et al. Tunable Strain in Magnetoelectric ZnO Microrod Composite Interfaces. *ACS Appl. Mater. Interfaces* **2017**, *9*, 25571–25577. [[CrossRef](#)] [[PubMed](#)]
37. Ding, M.; Zhao, D.; Yao, B.; E, S.; Guo, Z.; Zhang, L.; Shen, D. The ultraviolet laser from individual ZnO microwire with quadrate cross section. *Opt. Express* **2012**, *20*, 13657–13662. [[CrossRef](#)] [[PubMed](#)]
38. Li, Z.; Zhong, W.; Li, X.; Zeng, H.; Wang, G.; Wang, W.; Yang, Z.; Zhang, Y. Strong room-temperature ferromagnetism of pure ZnO nanostructure arrays via colloidal template. *J. Mater. Chem. C* **2013**, *1*, 6807–6812. [[CrossRef](#)]
39. Mishra, Y.K.; Mohapatra, S.; Singhal, R.; Avasthi, D.K.; Agarwal, D.C.; Ogale, S.B. Au–ZnO: A tunable localized surface plasmonic nanocomposite. *Appl. Phys. Lett.* **2008**, *92*, 43107. [[CrossRef](#)]
40. Mishra, Y.K.; Sören, K.; Arnim, S.; Ingo, P.; Xin, J.; Dawit, G.; Stefan, F.; Maria, C.; Sebastian, W.; Alexander, K.; et al. Fabrication of Macroscopically Flexible and Highly Porous 3D Semiconductor Networks from Interpenetrating Nanostructures by a Simple Flame Transport Approach. *Part. Part. Syst. Charact.* **2013**, *30*, 775–783. [[CrossRef](#)]
41. Yi, G.-C.; Wang, C.; Park, W.I. ZnO nanorods: Synthesis, characterization and applications. *Semiconduct. Sci. Technol.* **2005**, *20*, S22. [[CrossRef](#)]
42. Xu, S.; Wang, Z.L. One-dimensional ZnO nanostructures: Solution growth and functional properties. *Nano Res.* **2011**, *4*, 1013–1098. [[CrossRef](#)]
43. Reeber, R.R. Lattice parameters of ZnO from 4.2° to 296°K. *J. Appl. Phys.* **1970**, *41*, 5063–5066. [[CrossRef](#)]
44. Guo, Z.; Zhao, D.; Liu, Y.; Shen, D.; Zhang, J.; Li, B. Visible and ultraviolet light alternative photodetector based on ZnO nanowire/n-Si heterojunction. *Appl. Phys. Lett.* **2008**, *93*, 163501. [[CrossRef](#)]
45. Xu, C.X.; Sun, X.W. Field emission from zinc oxide nanopins. *Appl. Phys. Lett.* **2003**, *83*, 3806–3808. [[CrossRef](#)]
46. Gao, P.X.; Ding, Y.; Wang, Z.L. Crystallographic Orientation-Aligned ZnO Nanorods Grown by a Tin Catalyst. *Nano Lett.* **2003**, *3*, 1315–1320. [[CrossRef](#)]
47. Lee, C.J.; Lee, T.J.; Lyu, S.C.; Zhang, Y.; Ruh, H.; Lee, H.J. Field emission from well-aligned zinc oxide nanowires grown at low temperature. *Appl. Phys. Lett.* **2002**, *81*, 3648–3650. [[CrossRef](#)]
48. Xu, X.Y.; Zhang, H.Z.; Zhao, Q.; Chen, Y.F.; Xu, J.; Yu, D.P. Patterned Growth of ZnO Nanorod Arrays on a Large-Area Stainless Steel Grid. *J. Phys. Chem. B* **2005**, *109*, 1699–1702. [[CrossRef](#)] [[PubMed](#)]
49. Zhu, Z.; Chen, T.-L.; Gu, Y.; Warren, J.; Osgood, R.M. Zinc Oxide Nanowires Grown by Vapor-Phase Transport Using Selected Metal Catalysts: A Comparative Study. *Chem. Mater.* **2005**, *17*, 4227–4234. [[CrossRef](#)]
50. Yang, Y.H.; Wang, C.X.; Wang, B.; Li, Z.Y.; Chen, J.; Chen, D.H.; Xu, N.S.; Yang, G.W.; Xu, J.B. Radial ZnO nanowire nucleation on amorphous carbons. *Appl. Phys. Lett.* **2005**, *87*, 183109. [[CrossRef](#)]
51. Vayssieres, L.; Keis, K.; Lindquist, S.-E.; Hagfeldt, A. Purpose-Built Anisotropic Metal Oxide Material: 3D Highly Oriented Microrod Array of ZnO. *J. Phys. Chem. B* **2001**, *105*, 3350–3352. [[CrossRef](#)]
52. Greene, L.E.; Law, M.; Goldberger, J.; Kim, F.; Johnson, J.C.; Zhang, Y.; Saykally, R.J.; Yang, P. Low-Temperature Wafer-Scale Production of ZnO Nanowire Arrays. *Angew. Chem. Int. Ed.* **2003**, *42*, 3031–3034. [[CrossRef](#)] [[PubMed](#)]
53. Chen, S.-W.; Wu, J.-M. Nucleation mechanisms and their influences on characteristics of ZnO nanorod arrays prepared by a hydrothermal method. *Acta Mater.* **2011**, *59*, 841–847. [[CrossRef](#)]
54. Manekkathodi, A.; Lu, M.-Y.; Wang, C.W.; Chen, L.-J. Direct Growth of Aligned Zinc Oxide Nanorods on Paper Substrates for Low-Cost Flexible Electronics. *Adv. Mater.* **2010**, *22*, 4059–4063. [[CrossRef](#)] [[PubMed](#)]
55. Na, J.-S.; Gong, B.; Scarel, G.; Parsons, G.N. Surface Polarity Shielding and Hierarchical ZnO Nano-Architectures Produced Using Sequential Hydrothermal Crystal Synthesis and Thin Film Atomic Layer Deposition. *ACS Nano* **2009**, *3*, 3191–3199. [[CrossRef](#)] [[PubMed](#)]
56. Greene, L.E.; Yuhas, B.D.; Law, M.; Zitoun, D.; Yang, P. Solution-Grown Zinc Oxide Nanowires. *Inorg. Chem.* **2006**, *45*, 7535–7543. [[CrossRef](#)] [[PubMed](#)]
57. Sun, X.M.; Chen, X.; Deng, Z.X.; Li, Y.D. A CTAB-assisted hydrothermal orientation growth of ZnO nanorods. *Mater. Chem. Phys.* **2003**, *78*, 99–104. [[CrossRef](#)]

58. Zeng, H.; Cui, J.; Cao, B.; Gibson, U.; Bando, Y.; Golberg, D. Electrochemical Deposition of ZnO Nanowire Arrays: Organization, Doping, and Properties. *Sci. Adv. Mater.* **2010**, *2*, 336–358. [[CrossRef](#)]
59. Weintraub, B.; Zhou, Z.; Li, Y.; Deng, Y. Solution synthesis of one-dimensional ZnO nanomaterials and their applications. *Nanoscale* **2010**, *2*, 1573–1587. [[CrossRef](#)] [[PubMed](#)]
60. Tang, Y.; Luo, L.; Chen, Z.; Jiang, Y.; Li, B.; Jia, Z.; Xu, L. Electrodeposition of ZnO nanotube arrays on TCO glass substrates. *Electrochem. Commun.* **2007**, *9*, 289–292. [[CrossRef](#)]
61. Khajavi, M.R.; Blackwood, D.J.; Cabanero, G.; Tena-Zaera, R. New insight into growth mechanism of ZnO nanowires electrodeposited from nitrate-based solutions. *Electrochim. Acta* **2012**, *69*, 181–189. [[CrossRef](#)]
62. Xu, L.; Guo, Y.; Liao, Q.; Zhang, J.; Xu, D. Morphological Control of ZnO Nanostructures by Electrodeposition. *J. Phys. Chem. B* **2005**, *109*, 13519–13522. [[CrossRef](#)] [[PubMed](#)]
63. Wong, M.H.; Berenov, A.; Qi, X.; Kappers, M.J.; Barber, Z.H.; Illy, B.; Lockman, Z.; Ryan, M.P.; MacManus-Driscoll, J.L. Electrochemical growth of ZnO nano-rods on polycrystalline Zn foil. *Nanotechnology* **2003**, *14*, 968. [[CrossRef](#)]
64. Cao, B.; Li, Y.; Duan, G.; Cai, W. Growth of ZnO Nanoneedle Arrays with Strong Ultraviolet Emissions by an Electrochemical Deposition Method. *Cryst. Growth Des.* **2006**, *6*, 1091–1095. [[CrossRef](#)]
65. Mari, B.; Mollar, M.; Mechkour, A.; Hartiti, B.; Perales, M.; Cembrero, J. Optical properties of nanocolumnar ZnO crystals. *Microelectron. J.* **2004**, *35*, 79–82. [[CrossRef](#)]
66. Tena-Zaera, R.; Elias, J.; Wang, G.; Lévy-Clément, C. Role of Chloride Ions on Electrochemical Deposition of ZnO Nanowire Arrays from O₂ Reduction. *J. Phys. Chem. C* **2007**, *111*, 16706–16711. [[CrossRef](#)]
67. Elias, J.; Tena-Zaera, R.; Lévy-Clément, C. Effect of the Chemical Nature of the Anions on the Electrodeposition of ZnO Nanowire Arrays. *J. Phys. Chem. C* **2008**, *112*, 5736–5741. [[CrossRef](#)]
68. Yi, J.B.; Pan, H.; Lin, J.Y.; Ding, J.; Feng, Y.P.; Thongmee, S.; Liu, T.; Gong, H.; Wang, L. Ferromagnetism in ZnO Nanowires Derived from Electro-deposition on AAO Template and Subsequent Oxidation. *Adv. Mater.* **2008**, *20*, 1170–1174. [[CrossRef](#)]
69. Zheng, M.J.; Zhang, L.D.; Li, G.H.; Shen, W.Z. Fabrication and optical properties of large-scale uniform zinc oxide nanowire arrays by one-step electrochemical deposition technique. *Chem. Phys. Lett.* **2002**, *363*, 123–128. [[CrossRef](#)]
70. Li, Y.; Meng, G.W.; Zhang, L.D.; Phillipp, F. Ordered semiconductor ZnO nanowire arrays and their photoluminescence properties. *Appl. Phys. Lett.* **2000**, *76*, 2011–2013. [[CrossRef](#)]
71. Leprince-Wang, Y.; Bouchaib, S.; Brouri, T.; Capo-Chichi, M.; Laurent, K.; Leopoldes, J.; Tusseau-Nenez, S.; Lei, L.; Chen, Y. Fabrication of ZnO micro- and nano-structures by electrodeposition using nanoporous and lithography defined templates. *Mater. Sci. Eng. B* **2010**, *170*, 107–112. [[CrossRef](#)]
72. Zhou, H.; Wong, S.S. A Facile and Mild Synthesis of 1-D ZnO, CuO, and α -Fe₂O₃ Nanostructures and Nanostructured Arrays. *ACS Nano* **2008**, *2*, 944–958. [[CrossRef](#)] [[PubMed](#)]
73. Song, J.; Ning, X.; Zeng, H. ZnO nanowire lines and bundles: Template-deformation-guided alignment for patterned field-electron emitters. *Curr. Appl. Phys.* **2015**, *15*, 1296–1302. [[CrossRef](#)]
74. Sun, X.W.; Ling, B.; Zhao, J.L.; Tan, S.T.; Yang, Y.; Shen, Y.Q.; Dong, Z.L.; Li, X.C. Ultraviolet emission from a ZnO rod homojunction light-emitting diode. *Appl. Phys. Lett.* **2009**, *95*, 133124. [[CrossRef](#)]
75. Chang, C.-Y.; Tsao, F.-C.; Pan, C.-J.; Chi, G.-C.; Wang, H.-T.; Chen, J.-J.; Ren, F.; Norton, D.P.; Pearton, S.J.; Chen, K.-H.; et al. Electroluminescence from ZnO nanowire/polymer composite *p-n* junction. *Appl. Phys. Lett.* **2006**, *88*, 173503. [[CrossRef](#)]
76. Zhang, X.-M.; Lu, M.-Y.; Zhang, Y.; Chen, L.-J.; Wang, Z.L. Fabrication of a High-Brightness Blue-Light-Emitting Diode Using a ZnO-Nanowire Array Grown on *p*-GaN Thin Film. *Adv. Mater.* **2009**, *21*, 2767–2770. [[CrossRef](#)]
77. Tang, X.; Li, G.; Zhou, S. Ultraviolet Electroluminescence of Light-Emitting Diodes Based on Single *n*-ZnO/*p*-AlGaIn Heterojunction Nanowires. *Nano Lett.* **2013**, *13*, 5046–5050. [[CrossRef](#)] [[PubMed](#)]
78. Lupan, O.; Pauporté, T.; Viana, B. Low-Voltage UV-Electroluminescence from ZnO-Nanowire Array/*p*-GaIn Light-Emitting Diodes. *Adv. Mater.* **2010**, *22*, 3298–3302. [[CrossRef](#)] [[PubMed](#)]
79. Lupan, O.; Pauporté, T.; Viana, B.; Tiginyanu, I.M.; Ursaki, V.V.; Cortès, R. Epitaxial Electrodeposition of ZnO Nanowire Arrays on *p*-GaIn for Efficient UV-Light-Emitting Diode Fabrication. *ACS Appl. Mater. Interfaces* **2010**, *2*, 2083–2090. [[CrossRef](#)]
80. An, S.J.; Yi, G.-C. Near ultraviolet light emitting diode composed of *n*-GaIn/ZnO coaxial nanorod heterostructures on a *p*-GaIn layer. *Appl. Phys. Lett.* **2007**, *91*, 123109. [[CrossRef](#)]

81. Lee, S.W.; Cho, H.D.; Panin, G.; Kang, T.W. Vertical ZnO nanorod/Si contact light-emitting diode. *Appl. Phys. Lett.* **2011**, *98*, 93110. [[CrossRef](#)]
82. Zimmler, M.A.; Voss, T.; Ronning, C.; Capasso, F. Exciton-related electroluminescence from ZnO nanowire light-emitting diodes. *Appl. Phys. Lett.* **2009**, *94*, 241120. [[CrossRef](#)]
83. Liu, X.-Y.; Shan, C.-X.; Jiao, C.; Wang, S.-P.; Zhao, H.-F.; Shen, D.-Z. Pure ultraviolet emission from ZnO nanowire-based *p-n* heterostructures. *Opt. Lett.* **2014**, *39*, 422–425. [[CrossRef](#)] [[PubMed](#)]
84. Wang, J.-Y.; Lee, C.-Y.; Chen, Y.-T.; Chen, C.-T.; Chen, Y.-L.; Lin, C.-F.; Chen, Y.-F. Double side electroluminescence from *p-NiO/n-ZnO* nanowire heterojunctions. *Appl. Phys. Lett.* **2009**, *95*, 131117. [[CrossRef](#)]
85. Sun, X.W.; Huang, J.Z.; Wang, J.X.; Xu, Z. A ZnO Nanorod Inorganic/Organic Heterostructure Light-Emitting Diode Emitting at 342 nm. *Nano Lett.* **2008**, *8*, 1219–1223. [[CrossRef](#)] [[PubMed](#)]
86. Zhao, S.-L.; Kan, P.-Z.; Xu, Z.; Kong, C.; Wang, D.-W.; Yan, Y.; Wang, Y.-S. Electroluminescence of ZnO nanorods/MEH-PPV heterostructure devices. *Org. Electron.* **2010**, *11*, 789–793. [[CrossRef](#)]
87. Ren, X.; Zhang, X.; Liu, N.; Wen, L.; Ding, L.; Ma, Z.; Su, J.; Li, L.; Han, J.; Gao, Y. White Light-Emitting Diode From Sb-Doped *p-ZnO* Nanowire Arrays/*n-GaN* Film. *Adv. Funct. Mater.* **2015**, *25*, 2182–2188. [[CrossRef](#)]
88. Sun, H.; Zhang, Q.-F.; Wu, J.-L. Electroluminescence from ZnO nanorods with an *n-ZnO/p-Si* heterojunction structure. *Nanotechnology* **2006**, *17*, 2271. [[CrossRef](#)]
89. Huang, J.; Chu, S.; Kong, J.; Zhang, L.; Schwarz, C.M.; Wang, G.; Chernyak, L.; Chen, Z.; Liu, J. ZnO *p-n* Homo Junction Random Laser Diode Based on Nitrogen-Doped *p*-type Nanowires. *Adv. Opt. Mater.* **2013**, *1*, 179–185. [[CrossRef](#)]
90. Zhang, J.-Y.; Zhang, Q.-F.; Deng, T.-S.; Wu, J.-L. Electrically driven ultraviolet lasing behavior from phosphorus-doped *p-ZnO* nanonail array/*n-Si* heterojunction. *Appl. Phys. Lett.* **2009**, *95*, 211107. [[CrossRef](#)]
91. Zhang, J.-Y.; Li, P.-J.; Sun, H.; Shen, X.; Deng, T.-S.; Zhu, K.-T.; Zhang, Q.-F.; Wu, J.-L. Ultraviolet electroluminescence from controlled arsenic-doped ZnO nanowire homo junctions. *Appl. Phys. Lett.* **2008**, *93*, 21116. [[CrossRef](#)]
92. Yang, Y.; Sun, X.W.; Tay, B.K.; You, G.F.; Tan, S.T.; Teo, K.L. A *p-n* homo junction ZnO nanorod light-emitting diode formed by As ion implantation. *Appl. Phys. Lett.* **2008**, *93*, 253107. [[CrossRef](#)]
93. Chu, S.; Wang, G.; Zhou, W.; Lin, Y.; Chernyak, L.; Zhao, J.; Kong, J.; Li, L.; Ren, J.; Liu, J. Electrically pumped waveguide lasing from ZnO nanowires. *Nat. Nanotechnol.* **2011**, *6*, 506–510. [[CrossRef](#)] [[PubMed](#)]
94. Gao, F.; Zhang, D.; Wang, J.; Sun, H.; Yin, Y.; Sheng, Y.; Yan, S.; Yan, B.; Sui, C.; Zheng, Y.; et al. Ultraviolet electroluminescence from Au-ZnO nanowire Schottky type light-emitting diodes. *Appl. Phys. Lett.* **2016**, *108*, 261103. [[CrossRef](#)]
95. Liu, W.Z.; Xu, H.Y.; Ma, J.G.; Liu, C.Y.; Liu, Y.X.; Liu, Y.C. Effect of oxygen-related surface adsorption on the efficiency and stability of ZnO nanorod array ultraviolet light-emitting diodes. *Appl. Phys. Lett.* **2012**, *100*, 203101. [[CrossRef](#)]
96. Liu, W.; Xu, H.; Yan, S.; Zhang, C.; Wang, L.; Wang, C.; Yang, L.; Wang, X.; Zhang, L.; Wang, J.; et al. Effect of SiO₂ Spacer-Layer Thickness on Localized Surface Plasmon-Enhanced ZnO Nanorod Array LEDs. *ACS Appl. Mater. Interfaces* **2016**, *8*, 1653–1660. [[CrossRef](#)] [[PubMed](#)]
97. Liu, C.Y.; Xu, H.Y.; Ma, J.G.; Li, X.H.; Zhang, X.T.; Liu, Y.C.; Mu, R. Electrically pumped near-ultraviolet lasing from ZnO/MgO core/shell nanowires. *Appl. Phys. Lett.* **2011**, *99*, 63115. [[CrossRef](#)]
98. Liu, W.Z.; Xu, H.Y.; Wang, C.L.; Zhang, L.X.; Zhang, C.; Sun, S.Y.; Ma, J.G.; Zhang, X.T.; Wang, J.N.; Liu, Y.C. Enhanced ultraviolet emission and improved spatial distribution uniformity of ZnO nanorod array light-emitting diodes via Ag nanoparticles decoration. *Nanoscale* **2013**, *5*, 8634–8639. [[CrossRef](#)] [[PubMed](#)]
99. Lu, J.; Shi, Z.; Wang, Y.; Lin, Y.; Zhu, Q.; Tian, Z.; Dai, J.; Wang, S.; Xu, C. Plasmon-enhanced Electrically Light-emitting from ZnO Nanorod Arrays/*p-GaN* Heterostructure Devices. *Sci. Rep.* **2016**, *6*, 25645. [[CrossRef](#)] [[PubMed](#)]
100. Zhang, C.; Marvinney, C.E.; Xu, H.Y.; Liu, W.Z.; Wang, C.L.; Zhang, L.X.; Wang, J.N.; Ma, J.G.; Liu, Y.C. Enhanced waveguide-type ultraviolet electroluminescence from ZnO/MgZnO core/shell nanorod array light-emitting diodes via coupling with Ag nanoparticles localized surface plasmons. *Nanoscale* **2015**, *7*, 1073–1080. [[CrossRef](#)] [[PubMed](#)]
101. Wang, D.-W.; Zhao, S.-L.; Xu, Z.; Kong, C.; Gong, W. The improvement of near-ultraviolet electroluminescence of ZnO nanorods/MEH-PPV heterostructure by using a ZnS buffer layer. *Org. Electron.* **2011**, *12*, 92–97. [[CrossRef](#)]

102. Fang, X.; Wei, Z.; Yang, Y.; Chen, R.; Li, Y.; Tang, J.; Fang, D.; Jia, H.; Wang, D.; Fan, J.; et al. Ultraviolet Electroluminescence from ZnS@ZnO Core–Shell Nanowires/*p*-GaN Introduced by Exciton Localization. *ACS Appl. Mater. Interfaces* **2016**, *8*, 1661–1666. [[CrossRef](#)] [[PubMed](#)]
103. Wang, C.; Bao, R.; Zhao, K.; Zhang, T.; Dong, L.; Pan, C. Enhanced emission intensity of vertical aligned flexible ZnO nanowire/*p*-polymer hybridized LED array by piezo-phototronic effect. *Nano Energy* **2015**, *14*, 364–371. [[CrossRef](#)]
104. Yang, Q.; Liu, Y.; Pan, C.; Chen, J.; Wen, X.; Wang, Z.L. Largely Enhanced Efficiency in ZnO Nanowire/*p*-Polymer Hybridized Inorganic/Organic Ultraviolet Light-Emitting Diode by Piezo-Phototronic Effect. *Nano Lett.* **2013**, *13*, 607–613. [[CrossRef](#)] [[PubMed](#)]
105. Sharma, P.; Sreenivas, K.; Rao, K.V. Analysis of ultraviolet photoconductivity in ZnO films prepared by unbalanced magnetron sputtering. *J. Appl. Phys.* **2003**, *93*, 3963–3970. [[CrossRef](#)]
106. Peng, L.; Hu, L.; Fang, X. Low-Dimensional Nanostructure Ultraviolet Photodetectors. *Adv. Mater.* **2013**, *25*, 5321–5328. [[CrossRef](#)] [[PubMed](#)]
107. Cheng, G.; Wu, X.; Liu, B.; Li, B.; Zhang, X.; Du, Z. ZnO nanowire Schottky barrier ultraviolet photodetector with high sensitivity and fast recovery speed. *Appl. Phys. Lett.* **2011**, *99*, 203105. [[CrossRef](#)]
108. Flemban, T.H.; Haque, M.A.; Aja, I.; Alwadai, N.; Mitra, S.; Wu, T.; Roqan, I.S. A Photodetector Based on *p*-Si/*n*-ZnO Nanotube Heterojunctions with High Ultraviolet Responsivity. *ACS Appl. Mater. Interfaces* **2017**, *9*, 37120–37127. [[CrossRef](#)] [[PubMed](#)]
109. Cho, H.D.; Zakirov, A.S.; Yuldashev, S.U.; Ahn, C.W.; Yeo, Y.K.; Kang, T.W. Photovoltaic device on a single ZnO nanowire *p*-*n* homojunction. *Nanotechnology* **2012**, *23*, 115401. [[CrossRef](#)] [[PubMed](#)]
110. Wang, L.; Zhao, D.; Su, Z.; Fang, F.; Li, B.; Zhang, Z.; Shen, D.; Wang, X. High spectrum selectivity organic/inorganic hybrid visible-blind ultraviolet photodetector based on ZnO nanorods. *Org. Electron.* **2010**, *11*, 1318–1322. [[CrossRef](#)]
111. Kind, H.; Yan, H.; Messer, B.; Law, M.; Yang, P. Nanowire Ultraviolet Photodetectors and Optical Switches. *Adv. Mater.* **2002**, *14*, 158–160. [[CrossRef](#)]
112. Hu, Y.; Zhou, J.; Yeh, P.-H.; Li, Z.; Wei, T.-Y.; Wang, Z.L. Supersensitive, Fast-Response Nanowire Sensors by Using Schottky Contacts. *Adv. Mater.* **2010**, *22*, 3327–3332. [[CrossRef](#)] [[PubMed](#)]
113. Zhou, J.; Gu, Y.; Hu, Y.; Mai, W.; Yeh, P.-H.; Bao, G.; Sood, A.K.; Polla, D.L.; Wang, Z.L. Gigantic enhancement in response and reset time of ZnO UV nanosensor by utilizing Schottky contact and surface functionalization. *Appl. Phys. Lett.* **2009**, *94*, 191103. [[CrossRef](#)] [[PubMed](#)]
114. Fu, X.-W.; Liao, Z.-M.; Zhou, Y.-B.; Wu, H.-C.; Bie, Y.-Q.; Xu, J.; Yu, D.-P. Graphene/ZnO nanowire/graphene vertical structure based fast-response ultraviolet photodetector. *Appl. Phys. Lett.* **2012**, *100*, 223114. [[CrossRef](#)]
115. Nie, B.; Hu, J.-G.; Luo, L.-B.; Xie, C.; Zeng, L.-H.; Lv, P.; Li, F.-Z.; Jie, J.-S.; Feng, M.; Wu, C.-Y.; et al. Monolayer Graphene Film on ZnO Nanorod Array for High-Performance Schottky Junction Ultraviolet Photodetectors. *Small* **2013**, *9*, 2872–2879. [[CrossRef](#)] [[PubMed](#)]
116. Panigrahi, S.; Basak, D. Solution-processed novel core-shell *n*-*p* heterojunction and its ultrafast UV photodetection properties. *RSC Adv.* **2012**, *2*, 11963–11968. [[CrossRef](#)]
117. Leung, Y.H.; He, Z.B.; Luo, L.B.; Tsang, C.H.A.; Wong, N.B.; Zhang, W.J.; Lee, S.T. ZnO nanowires array *p*-*n* homojunction and its application as a visible-blind ultraviolet photodetector. *Appl. Phys. Lett.* **2010**, *96*, 53102. [[CrossRef](#)]
118. Hatch, S.M.; Briscoe, J.; Dunn, S. A Self-Powered ZnO-Nanorod/CuSCN UV Photodetector Exhibiting Rapid Response. *Adv. Mater.* **2013**, *25*, 867–871. [[CrossRef](#)] [[PubMed](#)]
119. Wang, Y.; Chen, Y.; Zhao, W.; Ding, L.; Wen, L.; Li, H.; Jiang, F.; Su, J.; Li, L.; Liu, N.; et al. A Self-Powered Fast-Response Ultraviolet Detector of *p*-*n* Homo Junction Assembled from Two ZnO-Based Nanowires. *Nano-Micro Lett.* **2016**, *9*, 11. [[CrossRef](#)]
120. Bie, Y.Q.; Liao, Z.M.; Zhang, H.Z.; Li, G.R.; Ye, Y.; Zhou, Y.B.; Xu, J.; Qin, Z.X.; Dai, L.; Yu, D.P. Self-Powered, Ultrafast, Visible-Blind UV Detection and Optical Logical Operation based on ZnO/GaN Nanoscale *p*-*n* Junctions. *Adv. Mater.* **2011**, *23*, 649–653. [[CrossRef](#)] [[PubMed](#)]
121. Zhou, H.; Gui, P.; Yu, Q.; Mei, J.; Wang, H.; Fang, G. Self-powered, visible-blind ultraviolet photodetector based on *n*-ZnO nanorods/*i*-MgO/*p*-GaN structure light-emitting diodes. *J. Mater. Chem. C* **2015**, *3*, 990–994. [[CrossRef](#)]

122. Huang, H.; Fang, G.; Mo, X.; Yuan, L.; Zhou, H.; Wang, M.; Xiao, H.; Zhao, X. Zero-biased near-ultraviolet and visible photodetector based on ZnO nanorods/*n*-Si heterojunction. *Appl. Phys. Lett.* **2009**, *94*, 63512. [[CrossRef](#)]
123. Garnier, J.; Parize, R.; Appert, E.; Chaix-Pluchery, O.; Kaminski-Cachopo, A.; Consonni, V. Physical Properties of Annealed ZnO Nanowire/CuSCN Heterojunctions for Self-Powered UV Photodetectors. *ACS Appl. Mater. Interfaces* **2015**, *7*, 5820–5829. [[CrossRef](#)] [[PubMed](#)]
124. Lin, P.; Yan, X.; Zhang, Z.; Shen, Y.; Zhao, Y.; Bai, Z.; Zhang, Y. Self-Powered UV Photosensor Based on PEDOT:PSS/ZnO Micro/Nanowire with Strain-Modulated Photoresponse. *ACS Appl. Mater. Interfaces* **2013**, *5*, 3671–3676. [[CrossRef](#)] [[PubMed](#)]
125. Ni, P.-N.; Shan, C.-X.; Wang, S.-P.; Liu, X.-Y.; Shen, D.-Z. Self-powered spectrum-selective photodetectors fabricated from *n*-ZnO/*p*-NiO core-shell nanowire arrays. *J. Mater. Chem. C* **2013**, *1*, 4445–4449. [[CrossRef](#)]
126. Shen, Y.; Yan, X.; Bai, Z.; Zheng, X.; Sun, Y.; Liu, Y.; Lin, P.; Chen, X.; Zhang, Y. A self-powered ultraviolet photodetector based on solution-processed *p*-NiO/*n*-ZnO nanorod array heterojunction. *RSC Adv.* **2015**, *5*, 5976–5981. [[CrossRef](#)]
127. Chen, Z.; Li, B.; Mo, X.; Li, S.; Wen, J.; Lei, H.; Zhu, Z.; Yang, G.; Gui, P.; Yao, F.; et al. Self-powered narrowband *p*-NiO/*n*-ZnO nanowire ultraviolet photodetector with interface modification of Al₂O₃. *Appl. Phys. Lett.* **2017**, *110*, 123504. [[CrossRef](#)]
128. Yu, J.; Chen, X.; Wang, Y.; Zhou, H.; Xue, M.; Xu, Y.; Li, Z.; Ye, C.; Zhang, J.; van Aken, P.A.; et al. A high-performance self-powered broadband photodetector based on a CH₃NH₃PbI₃ perovskite/ZnO nanorod array heterostructure. *J. Mater. Chem. C* **2016**, *4*, 7302–7308. [[CrossRef](#)]
129. Bai, Z.; Zhang, Y. Self-powered UV–visible photodetectors based on ZnO/Cu₂O nanowire/electrolyte heterojunctions. *J. Alloy. Compd.* **2016**, *675*, 325–330. [[CrossRef](#)]
130. Guo, Z.; Zhou, L.; Tang, Y.; Li, L.; Zhang, Z.; Yang, H.; Ma, H.; Nathan, A.; Zhao, D. Surface/Interface Carrier-Transport Modulation for Constructing Photon-Alternative Ultraviolet Detectors Based on Self-Bending-Assembled ZnO Nanowires. *ACS Appl. Mater. Interfaces* **2017**, *9*, 31042–31053. [[CrossRef](#)] [[PubMed](#)]
131. Lao, C.S.; Park, M.-C.; Kuang, Q.; Deng, Y.; Sood, A.K.; Polla, D.L.; Wang, Z.L. Giant Enhancement in UV Response of ZnO Nanobelts by Polymer Surface-Functionalization. *J. Am. Chem. Soc.* **2007**, *129*, 12096–12097. [[CrossRef](#)] [[PubMed](#)]
132. Liu, K.; Sakurai, M.; Liao, M.; Aono, M. Giant Improvement of the Performance of ZnO Nanowire Photodetectors by Au Nanoparticles. *J. Phys. Chem. C* **2010**, *114*, 19835–19839. [[CrossRef](#)]
133. Gogurla, N.; Sinha, A.K.; Santra, S.; Manna, S.; Ray, S.K. Multifunctional Au-ZnO Plasmonic Nanostructures for Enhanced UV Photodetector and Room Temperature NO Sensing Devices. *Sci. Rep.* **2014**, *4*, 6483. [[CrossRef](#)] [[PubMed](#)]
134. Zeng, Y.; Pan, X.; Lu, B.; Ye, Z. Fabrication of flexible self-powered UV detectors based on ZnO nanowires and the enhancement by the decoration of Ag nanoparticles. *RSC Adv.* **2016**, *6*, 31316–31322. [[CrossRef](#)]
135. Tzeng, S.-K.; Hon, M.-H.; Leu, I.-C. Improving the Performance of a Zinc Oxide Nanowire Ultraviolet Photodetector by Adding Silver Nanoparticles. *J. Electrochem. Soc.* **2012**, *159*, H440–H443. [[CrossRef](#)]
136. Zhao, X.; Wang, F.; Shi, L.; Wang, Y.; Zhao, H.; Zhao, D. Performance enhancement in ZnO nanowire based double Schottky-barrier photodetector by applying optimized Ag nanoparticles. *RSC Adv.* **2016**, *6*, 4634–4639. [[CrossRef](#)]
137. Lin, D.; Wu, H.; Zhang, W.; Li, H.; Pan, W. Enhanced UV photoresponse from heterostructured Ag–ZnO nanowires. *Appl. Phys. Lett.* **2009**, *94*, 172103. [[CrossRef](#)]
138. West, P.R.; Ishii, S.; Naik, G.V.; Emani, N.K.; Shalaev, V.M.; Boltasseva, A. Searching for better plasmonic materials. *Laser Photonics Rev.* **2010**, *4*, 795–808. [[CrossRef](#)]
139. Lu, J.; Xu, C.; Dai, J.; Li, J.; Wang, Y.; Lin, Y.; Li, P. Improved UV photoresponse of ZnO nanorod arrays by resonant coupling with surface plasmons of Al nanoparticles. *Nanoscale* **2015**, *7*, 3396–3403. [[CrossRef](#)] [[PubMed](#)]
140. Deka Boruah, B.; Misra, A. Effect of Magnetic Field on Photoresponse of Cobalt Integrated Zinc Oxide Nanorods. *ACS Appl. Mater. Interfaces* **2016**, *8*, 4771–4780. [[CrossRef](#)] [[PubMed](#)]
141. Su, Y.; Wu, Z.; Wu, X.; Long, Y.; Zhang, H.; Xie, G.; Du, X.; Tai, H.; Jiang, Y. Enhancing responsivity of ZnO nanowire based photodetectors by piezo-phototronic effect. *Sens. Actuators A Phys.* **2016**, *241*, 169–175. [[CrossRef](#)]

142. Lu, S.; Qi, J.; Liu, S.; Zhang, Z.; Wang, Z.; Lin, P.; Liao, Q.; Liang, Q.; Zhang, Y. Piezotronic Interface Engineering on ZnO/Au-Based Schottky Junction for Enhanced Photoresponse of a Flexible Self-Powered UV Detector. *ACS Appl. Mater. Interfaces* **2014**, *6*, 14116–14122. [[CrossRef](#)] [[PubMed](#)]
143. Zhang, Z.; Liao, Q.; Yu, Y.; Wang, X.; Zhang, Y. Enhanced photoresponse of ZnO nanorods-based self-powered photodetector by piezotronic interface engineering. *Nano Energy* **2014**, *9*, 237–244. [[CrossRef](#)]
144. Zhang, F.; Ding, Y.; Zhang, Y.; Zhang, X.L.; Wang, Z.L. Piezo-phototronic Effect Enhanced Visible and Ultraviolet Photodetection Using a ZnO-CdS Core-Shell Micro/nanowire. *ACS Nano* **2012**, *6*, 9229–9236. [[CrossRef](#)] [[PubMed](#)]
145. Liu, Y.; Yang, Q.; Zhang, Y.; Yang, Z.; Wang, Z.L. Nanowire Piezo-phototronic Photodetector: Theory and Experimental Design. *Adv. Mater.* **2012**, *24*, 1410–1417. [[CrossRef](#)] [[PubMed](#)]
146. Yang, Q.; Guo, X.; Wang, W.; Zhang, Y.; Xu, S.; Lien, D.H.; Wang, Z.L. Enhancing Sensitivity of a Single ZnO Micro-/Nanowire Photodetector by Piezo-phototronic Effect. *ACS Nano* **2010**, *4*, 6285–6291. [[CrossRef](#)] [[PubMed](#)]



© 2018 by the authors. Licensee MDPI, Basel, Switzerland. This article is an open access article distributed under the terms and conditions of the Creative Commons Attribution (CC BY) license (<http://creativecommons.org/licenses/by/4.0/>).